BLOOD RHEOLOGY:
PROPOSED MODELS AND THE EFFECTS OF CATION CONCENTRATION AND ACTIVE HYPEREMIA

Thesis for the Degree of Ph. D.
MICHIGAN STATE UNIVERSITY
JOSEPH G. MASIN
1971

This is to certify that the

thesis entitled

BLOOD RHEOLOGY:
PROPOSED MODELS AND THE EFFECTS OF
CATION CONCENTRATION AND ACTIVE HYPEREMIA

presented by

JOSEPH G. MASIN

has been accepted towards fulfillment
of the requirements for

Ph.D. degree in CHEMICAL ENGINEERING

Major professor D. ANDERSON

Date August 10, 1971

ABSTRACT

BLOOD RHEOLOGY: PROPOSED MODELS AND THE EFFECTS OF CATION CONCENTRATION AND ACTIVE HYPEREMIA

By

Joseph G. Masin

Two rheological models were investigated for their ability to describe the flow of blood, and the effects of both cation concentration and active hyperemia on blood viscosity were studied.

A couple stress model was proposed for blood by Valanis and Sun, but their model lacks a yield stress. This rheological feature has been demonstrated by many investigators in blood and must be included in any model which is to describe blood flow. A yield stress term was added to the couple stress model of Valanis and Sun and the mathematical results were found to be physically impossible. Therefore, their concept of a couple stress does not describe the rheology of blood.

Turbulence theory was applied to the flow of blood and it was concluded that momentum transport by the eddy-like rotation of red blood cells (RBC's) was negligible when compared to momentum transport by the laminar flow of a suspension of RBC's in plasma. At low shear rates, there were more particle-particle interactions than proposed by a simple yield stress fluid.

The best available rheological model for blood is the Casson model. It was used to investigate the effects on viscosity and yield stress of altered cation concentrations and of active hyperemia.

Joseph G. Masin

The concentration of the principal cations (sodium, potassium, calcium, magnesium, and hydrogen) in canine blood was altered by 1:7 dilution with various isotonic salt solutions differing in their ionic makeup. The resulting ionic concentrations in blood represented high, normal, and low physiological values. Total tonicity remained constant. Low pH (7.02) blood had a 0.019 dyne/cm^2 higher yield stress than control blood (pH 7.43) with a significance of less than 0.01. Control blood was a paired aliquot of blood diluted 1:7 with dialysate solution to maintain tonicity, other ionic concentrations, and hematocrit at the same level as the test sample. Blood viscosity increased 15.2% at a potassium ion concentration of 13.2 meq/l when compared with control blood (4.2 meq K^+/l). This change is significant at the 0.05 level. All other conditions tested produced no significant changes in either viscosity or yield stress. Venous outflow from a canine gracilis undergoing active hyperemia was not different in viscosity from the venous outflow prior to stimulation (6V, 6 sec^{-1}, .06 msec). However, the yield stress was an average of 0.028 dyne/cm^2 higher, which change is significant at the 0.01 level.

BLOOD RHEOLOGY:

PROPOSED MODELS AND THE EFFECTS OF

CATION CONCENTRATION AND ACTIVE HYPEREMIA

By

Joseph G. Masin

A THESIS

Submitted to
Michigan State University
in partial fulfillment of the requirements
for the degree of

DOCTOR OF PHILOSOPHY

Department of Chemical Engineering

1971

To my parents

and

my wife

ACKNOWLEDGMENTS

The guidance and encouragement of Dr. Donald K. Anderson were sincerely appreciated throughout the course of this study.

The patience of the author's wife, Carol, and her aid in the preparation of this manuscript were deeply appreciated.

The author is grateful for financial support received during his studies to the National Science Foundation and to the Department of Chemical Engineering and the Division of Engineering Research at Michigan State University.

The craftmanship and labors of the Mechanical Shop of the Division of Engineering Research were appreciated.

Photographic work was done by William D. Hamilton.

TABLE OF CONTENTS

Page

APPENDICES (Cont'd.)

LIST OF FIGURES

LIST OF TABLES

INTRODUCTION

The human body, its parts, and its functions have increasingly become objects for engineering study. It is only natural that the engineer, as a human being, should be concerned with trying to eliminate the suffering and aging that befall other humans. However, it has only been fairly recently that many engineers have seen that they can make contributions which are as useful as those made by the traditional healers. Several avenues of attack on health problems have been used and are particularly well suited to engineering study. One is modeling and computer studies, since the engineer is well trained in the mathematical and physical sciences. Another is the design of research equipment and laboratory apparatus. In this study, both of these avenues were employed--an apparatus was designed to measure pressure drop as a function of flow rate for blood, and two proposed rheological models were tested with the collected data.

The rheology of complex suspensions, such as blood, is not well understood. Blood is a suspension of erythrocytes (red blood cells or RBC's), leukocytes (white blood cells), and platelets in a solution called plasma. The components of normal plasma are shown in Table 1. The suspension usually consists of about forty-five volume percent (hematocrit or Hct) red blood cells, fifty-five percent plasma and small amounts of the other cells. Associated with many diseased or abnormal states is an altered ability of the blood to flow. Some cellular changes which affect viscosity are abnormal

TABLE 1

MAIN COMPONENTS OF NORMAL PLASMA [14, 4, 16]

	Range
PROTEINS	Total 6.0 - 8.0 gm/100ml
ALBUMIN	3.3 - 5.4 gm/100ml
GLOBULINS	1.6 - 3.4 gm/100ml
FIBRINOGEN	0.2 - 0.4 gm/100ml
OTHER SUBSTANCES	
LIPIDS	400 - 850 mg/100ml
GLUCOSE	70 - 170 mg/100ml
UREA	24 - 49 mg/100ml
ORGANIC ACIDS	3.5 - 7.7 mg/100ml
INORGANIC IONS	
SODIUM	313-334 mg/100ml, 136-145 mEq/l
POTASSIUM	14-20 mg/100ml, 3.58-5.12 mEq/l
CALCIUM	9-11.1 mg/100ml, 4.49-5.53 mEq/l
MAGNESIUM	1.8-3.0 mg/100ml, 1.48-2.47 mEq/l
CHLORIDE	352-375 mg/100ml, 99.3-106 mEq/l
BICARBONATE	130-170 mg/100ml, 21.3-27.8 mEq/l
PHOSPHATE	9.0-14.0mg/100ml, 1.88-2.98 mEq/l

shape, size, flexibility, and concentration of cells. Alterations in the plasma of the amounts of ions, proteins, or other substances are also associated with viscosity changes. This study is an investigation of the effects of abnormal concentrations of the potassium, magnesium, calcium, and hydrogen ions on the viscosity and yield stress of whole blood.

The organization of this study is to first consider the previous work concerning:

1) local ionic effects upon the resistance to blood flow,

2) the equipment and procedures used to gather data on these effects, and

3) the fluid models which aid in interpreting the data collected.

Next, the work done by this investigator will be described. Presented are:

1) two new fluid models and their applicability to blood rheology,

2) the equipment and procedures used in this study, and

3) the effects of cation concentration and active hyperemia on blood viscosity.

BACKGROUND

All animals above microscopic size rely on the circulation of blood to supply necessary raw materials and to remove waste products from each of the cells of that organism. There are many immediate and remote determinants of blood flow and some of these are shown in Figure 1. For almost one hundred fifty years, investigators have tried to derive equations which quantitatively describe the dependence of flow on each of the parameters shown. This science is now known as hemorheology.

IONIC EFFECTS

One parameter listed in Figure 1 is ions. Ions can affect viscosity by their individual presence (concentration) or by their collective presence (tonicity). They can also affect flow geometry via active radius alteration. The separation of in-vivo ionic effects into viscosity and geometry components is not easy and many investigators, for example, Roth [53], simply assumed any effects could be attributed to geometry alteration. An example showing there is an effect of ions on viscosity is the case of pH in vitro [48, 50, 69] where increased pH causes a marked increase in viscosity.

In vivo effects are harder to interpret. Locally decreased blood pH causes decreased resistance to flow through the mechanism of vasodilation [31, 56] while locally increased blood pH causes increased resistance to flow. However, non-blood perfusate yields

FIGURE 1
DETERMINANTS OF LOCAL BLOOD FLOW [30]

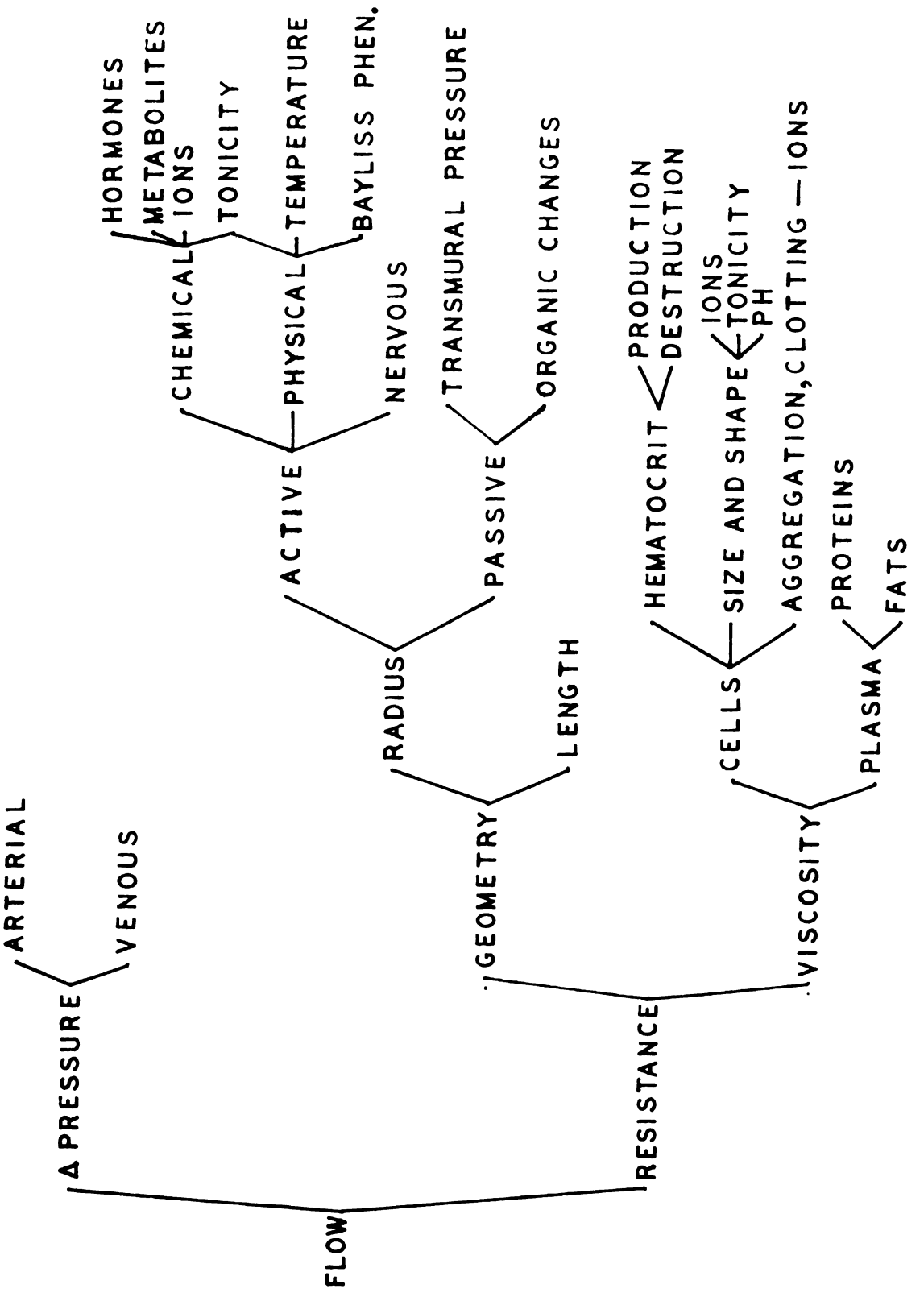

slightly different results [9], and there are inconclusive results of systemic pH effects [50].

The in vivo local effects of other ions have been summarized by Haddy and Scott [31, 56]. Potassium depletion or hypokalemia causes increased resistance to flow while mild hyperkalemia (16-32 mg/100 ml) causes decreased resistance. Hyperkalemia above 40 mg/100 ml causes increased resistance. Calcium depletion or hypocalcemia causes increased resistance. Increased magnesium concentration or hypermagnesemia causes decreased resistance, but the results from hypomagnesemia are inconclusive. There appears to be no effects from an excess or a depletion of sodium, chloride, bicarbonate, biphosphate, or sulfate ions. The acetate and citrate ions decrease resistance, perhaps via calcium binding.

The tonicity or osmolarity of blood also has an effect [31, 56]. Hypotonic (diluted) blood exhibits increased resistance to flow while hyperosmolar (concentrated) blood exhibits decreased resistance.

PREVIOUS EXPERIMENTAL PROCEDURES

To study the effects of ions and other parameters on the resistance to flow of blood, many different procedures and equipment designs have been used. The results and conclusions of much early work on blood rheology have had to be modified as scientific understanding has been applied to the original crude procedures.

Many early investigators, for example Fahraeus and Lindqvist [21], tried to mimic the system of interest, the body, by imposing the same pressure drop as the heart, 100 mm Hg, and measuring the resulting flow through an experimental capillary. Several problems developed with this system. Firstly, the appropriate pressure drop is not 100 mm Hg

but that pressure corrected for kinetic energy effects [49], and end, wall, and other effects [66]. Secondly, the meniscus movement used for flow measurement exerts a resistance of its own [36] which is quite considerable in small tubes and varies with direction of meniscus movement and degree of wall soil. Thirdly, blood settling in the apparatus may cause a varying hematocrit. Finally, the yield stress of blood cannot be detected at the high shear rates of this design, a factor which helped delay this important discovery.

Problems have also been discovered from the use of a rotational viscometer for blood rheology. First, blood settles in the cup since it is not adequately stirred. Second, blood proteins are attracted to the surface, form a layer, and cause varying results depending on the length of time the blood is in the apparatus. However, this difficulty can be overcome by the use of a guard ring [18, 28]. Third, since the centers of red blood cells physically cannot be within 1.5μ (one RBC width) of the rotating bob, there is a skimming effect which can be circumvented only through the use of a notched bob [13].

Since the systemic circulation contains roughly cylindrical capillaries and geometry dependent effects have been noticed, and since all objections to the capillary type apparatus can be removed by appropriate equipment design and mathematical treatment of the raw data, this type rheometer was used here. The treatment of pressure drop corrections can easily be accomplished by standard techniques using a calculator or computer. The problem of meniscal resistance was avoided by changing from a system in which flow was the measured or dependent variable and pressure was the determined or independent variable (a pressure-flow system). Instead a

a constant flow rate was established by a displacement type pump and the resulting pressure drop was measured (a flow-pressure system). Blood settling was avoided by stirring. Finally, selection of a low flow rate pump resulted in low pressure drops which allowed the yield stress to be determined.

Blood pH may be measured with any of the commercial meters. However, there is a small hematocrit-dependent error due to RBC polarization if bulb electrodes are used [17]. This was neglected in this study.

A major problem with experiments using blood is blood's tendency to clot soon after removal from the body. There are many anticoagulents available to eliminate this tendency. However some (like Red Cross acid-citrate dextrose solution or ACD) must be added in large volumes and this precludes study at physiological hematocrits. Studies [15, 37, 52] of other anticoagulents have shown that they alter blood viscosity. Heparin was used in this study because it is effective at low concentrations and does not alter viscosity [23].

FLUID MODELING OF BLOOD

Once data has been collected on a system of interest, fluid models aid in interpreting the data. The first attempt to mathematically describe data from the flow of blood in a tube was made by Poiseuille [22]. Experimental difficulties (clotting) forced a change of fluid to water and the famous Hagen-Poiseuille equation for the flow of a Newtonian fluid resulted.

$$Q = \Delta p \pi R^4 / 8 \mu L \qquad (1)$$

where Q is the flow rate, Δp is the pressure drop, R is the tube radius, μ is the fluid viscosity, and L is the length of tube considered.

Unfortunately, blood is not Newtonian and a few investigators soon reported that Equation 1 did not fit blood data. However, there was almost a century lapse before the first systematic study on blood was done to try to explain the observed deviations (non-Newtonian behavior). This study by Fahraeus and Lindqvist [21] showed a geometric dependence of viscosity in the form of a decrease in apparent viscosity as the viscometer tube diameter decreased towards body capillary size. Divers studies were undertaken thereafter, but, as late as 1959, Haynes and Burton [32] complained of the lack of comprehensive work on the rheology of blood. Even these researchers were largely empirical in their approach to the problem.

An important feature of blood rheology is the presence of a yield stress or non-zero intercept on a stress-strain rate recording. That is, the stress on blood must be greater than some positive number, called the yield stress, before there is any effect on the strain rate. This type behavior is called Bingham plastic if the stress is linear with strain rate. However, data for blood shows a non-linear relationship.

A constitutive equation based on the assumption of interacting chains of particles was proposed by Casson [10] for India ink and was applied to blood by Scott Blair [58]. The equation is

$$\tau^{\frac{1}{2}} = \tau_y^{\frac{1}{2}} + s\dot{\gamma}^{\frac{1}{2}} \qquad \tau \geq \tau_y \tag{2a}$$

$$0 = \dot{\gamma} \qquad \tau \leq \tau_y \tag{2b}$$

where τ is the shear stress, τ_y is the yield stress, s^2 is a coefficient of viscosity, and $\dot{\gamma}$ is the strain rate. For flow in a tube, $\dot{\gamma} = -dv/dr$. If Equation 2a is squared,

$$\tau = \tau_y + s^2\dot{\gamma} + 2s(\tau_y\dot{\gamma})^{\frac{1}{2}} \tag{3}$$

Equation 3 is equivalent to a Bingham plastic model with an additive cross term in the square roots. At high strain rates, the dominant term on the right hand side is the second and behavior is seemingly Newtonian. Thus s^2 may be called the limiting Newtonian viscosity for a Casson fluid.

Equation 2 has been found to describe the stress versus strain rate behavior of blood very well in both capillary and rotational viscometers. Current debate [11, 45] concerns whether there is a change to Newtonian behavior at high strain rate or whether Casson's equation is valid for all strain rates. Based on the acceptance of Casson's equation to describe data at the strain rates used in this study, it was used here to evaluate the effect of abnormal ion concentrations on blood flow.

If $\bar{U} = 4\,Q/\pi D^3$ is the average flow velocity in a tube in units of tube diameters per time and $\tau_w = \Delta_p D/4L$ is the shear stress at the tube wall, the Hagen-Poiseuille equation for flow of a Newtonian fluid can be written

$$\bar{U} = \tau_w/8\,\mu \tag{4}$$

while Bingham's model predicts

$$\bar{U} = (\tau_w/8 - \tau_y/6 + \tau_y^4/12\,\tau_w^3)\ /\mu \tag{5}$$

and Casson's model (see Appendix A) predicts

$$\bar{U} = (\tau_w/8 - 2\tau_w^{\frac{1}{2}}\tau_y^{\frac{1}{2}}/7 - \tau_y^4/168\tau_w^3 + \tau_y/6)/s^2 \tag{6}$$

Figure 2 shows the ability of each of these equations to fit data on the flow of whole blood in the range investigated.

There are several minor drawbacks in applying Casson's equation to blood flow. An extensive study by Benis [3] has shown that model

FIGURE 2
CASSON EQUATION FOR BLOOD FLOW

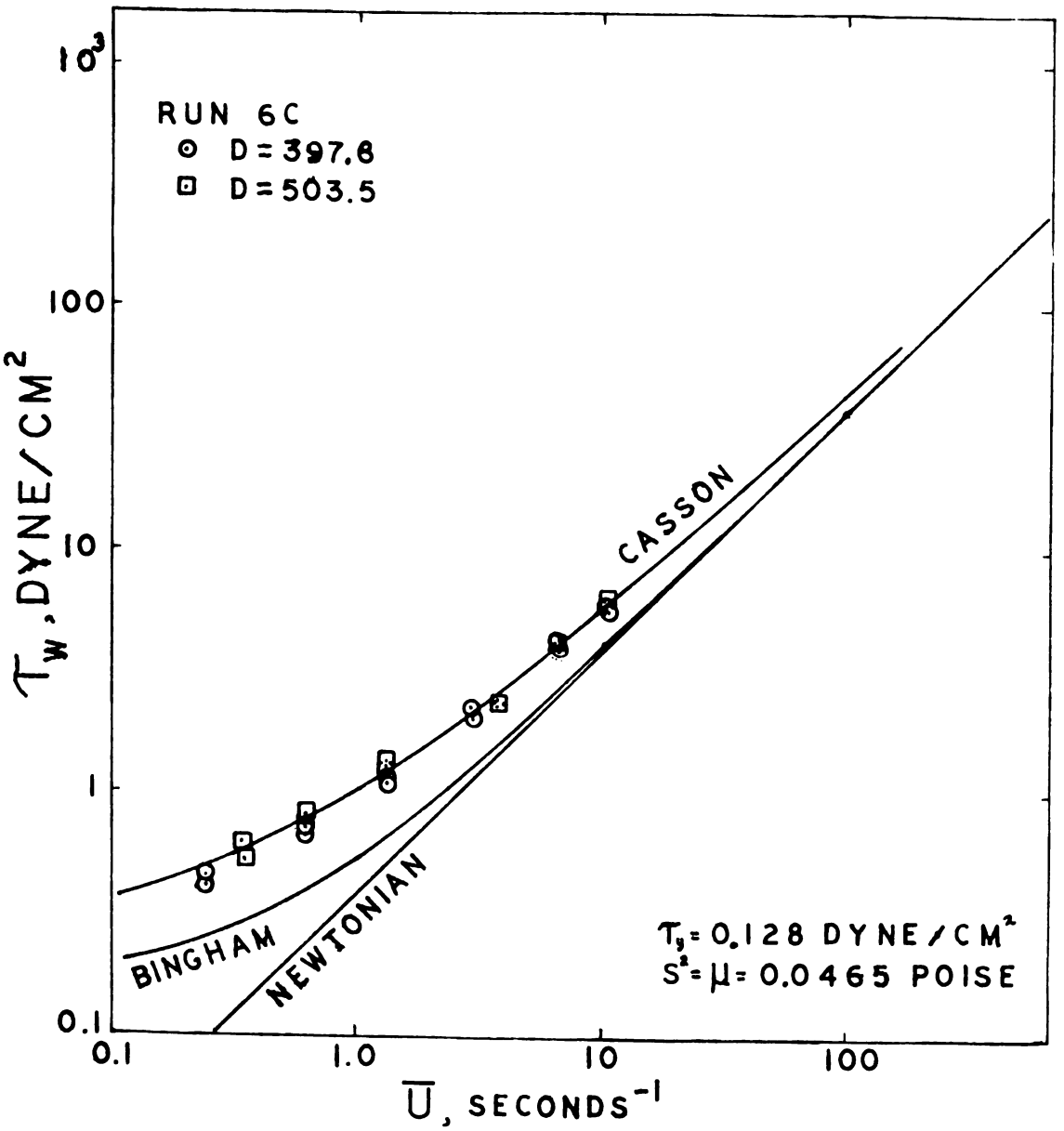

parameters still vary slightly with viscometer tube radius and that not all samples fit Casson's equation well. Also, the yield stress is a function of hematocrit [41] and fibrinogen concentration [42, 43], and therefore cannot be predicted without knowledge of blood composition.

One attempt to correct these drawbacks was a constitutive equation proposed by Valanis and Sun [63], which introduced the concept of a couple stress for blood.

This model has a radius dependent parameter, $\overline{\lambda}$, which may help explain the deviation noted by Benis. An unusual feature of the model is that the viscosity is not hematocrit dependent [65]. Of course, the ability of blood to flow changes extensively with hematocrit, as has been noted and charted by Haynes and Burton [32] and Whittaker and Winton [70]. To explain this change, Valanis and Sun have allowed one parameter, $\overline{\alpha}$, to vary with hematocrit, so this feature is really no improvement over Casson's equation. Some drawbacks of the model are that the dependence of flow rate on wall shear rate is linear and no provision has been made for the existence of a yield stress, both contrary to experimental data. An empirical modification of the model, based on the shear rate dependence of the Casson equation, removes the last two defects [38].

An equation utilizing both yield and couple stresses is developed in the theory section and its applicability to blood flow is evaluated.

FLUID MODELS

FLUID MODELS

Many models have been proposed for blood flow. The most successful is the Casson equation, which describes blood rheology well over a wide range of conditions. This model is based on the assumption of a suspension of interacting rods. The length to diameter ratio of the rods is assumed to be inversely proportional to the square root of the shear rate. Photographic studies of blood flow show that rouleaux, or stacked agglomerates of RBC's do exist in blood and are rodlike in appearance. However, the amount and size of these rouleaux do not correlate well with the proposed shear rate dependence.

Thus, despite the availability of an accurate model, other equations have been proposed, and will be proposed, in order both to explain blood rheology and to explain phenomena which are observed microscopically. The two models which are considered in detail in this section are

1. Poiseuille Flow of a Fluid with Couple and Yield Stresses and
2. The Fluid with Particulate Turbulence.

The first model investigated here utilizes the concept that a couple stress exists in blood. Valanis and Sun proposed this concept and found that published velocity profiles could be fit well with it. However, their equation involving the couple stress does not include a yield stress term in it, and this feature has been observed by many investigators in blood. Their model is modified here to include this feature so that both a couple stress and a yield stress exist in the fluid model.

The other model investigated here is turbulence theory applied to blood flow. Modifications are made to the normal turbulence theory to fit the nature of turbulence which would be due to RBC rotation. This allows the order of magnitude of momentum transport by this mechanism to be calculated compared with transport by laminar shear.

POISEUILLE FLOW OF A FLUID WITH COUPLE AND YIELD STRESSES

A fluid model using a couple stress in addition to the usual viscosity has been developed by Valanis and Sun [63]. They show in their paper that data on the velocity profile of blood in a tube can be fit to their equation if high shear rates are involved. Their model must fail to describe blood at low shear rates since their shear stress is linear and homogeneous with strain rate. A yield stress must be included in the fluid model if it is to describe blood.

Explanation of the concept of a couple stress is needed since, by the following reasoning, it cannot exist in a continuum [20]. If the couple stress is confined in a volume element and the size of the volume element is allowed to go to zero, the length of the lever arm of the couple must go to zero. Then the existence of a finite couple requires that the parallel forces of the couple must become infinite, which is not tractable. However, in a fluid such as blood, which is discontinuous even on the microscopic scale due to the presence of red blood cells and other particulate matter, this limiting process cannot be performed and the concept of a couple stress is feasible. The rigidity of the formed matter in blood causes a drag resisting the shear forces. This drag varies over the surface of the rigid body and results in a net couple which is finite and volume dependent, since as the volume goes to zero,

the drag also disappears. This intuitive picture of the couple stress as a drag force which arises to resist shear is in accord with Stokes' [61] conclusion from analyzing the equations of motion that a shear stress field is necessary in order for a couple stress to be possible.

Appendix A gives the mathematical derivation of the velocity profile using the fluid model with couple and yield stresses. The resulting equation is derived as A74.

$$v = \frac{\tau_w R}{2s^2}\left[1 - (r/R)^2 + A\,(I_0(\alpha r/R) - I_0(\alpha))\right]$$

$$- \frac{\tau_y R}{s^2}\left[1 - r/R + \frac{\pi}{2}\,(L_0(\alpha r/R) - L_0(\alpha)\right.$$

$$\left. - B(I_0(\alpha r/R) - I_0(\alpha))\right] \qquad \text{for } \tau \geq \tau_y \qquad (7a)$$

$$v = \text{constant} \qquad \text{for } \tau < \tau_y \qquad (7b)$$

where

$$A = \frac{2(1-\bar{\eta})}{\alpha^2\,(I_0(\alpha) - (1+\bar{\eta})\,I_1(\alpha)/\alpha)} \qquad (7c)$$

and

$$B = \left[L_0(\alpha) - (1+\bar{\eta})\,L_1(\alpha)/\alpha\right] / \left[I_0(\alpha) - (1+\bar{\eta})\,I_1(\alpha)/\alpha\right]. \qquad (7d)$$

It is desired to determine if this equation follows the correct limiting process as the shear stress at the wall falls to the yield stress. There have been several studies made, for example by Merrill, et al [43, 45], which show that the yield stress as determined by extrapolation of wall shear stress from pressure-flow data is identical with the value of the yield stress as determined from static tests. Therefore, flow must go to zero as the shear stress at the wall goes to the yield stress. There are two possible ways for this to occur. Firstly, the velocity might go to zero at all radii, as occurs when a Newtonian fluid approaches its lower limit of shear stress = zero. Secondly, there might exist a plug flow region which grows in size and the plug velocity might go to zero, as occurs when a Bingham fluid approaches its lower limit of shear stress = yield stress.

In this case, if the appropriate derivative is formed, from Equation 7

$$dv/dr = I_1 (\alpha r/R) \left[(1 - \bar{\eta}) \tau_w/\alpha + \bar{\eta} \tau_y (L_0(\alpha) - (1 + \bar{\eta}) L_1(\alpha)/\alpha)/2\right] / \left[s^2 (I_0(\alpha) - (1 + \bar{\eta}) I_1(\alpha)/\alpha)\right] - \left[\tau_w r/R + L_1(\alpha r/R) \bar{\eta} \tau_y/2\right] / s^2 \quad (8)$$

it is clear that, in general, dv/dr is not zero at the yield radius, $r_y = R \tau_y/\tau_w$. Therefore, the same plug region does not exist for this model as the Bingham model, and the regional distinction implied by Equation 7a and b is incorrect since then the velocity gradient would be discontinuous.

The velocity profile across the tube for some values of α and for the range of permissible $\bar{\eta}$ values is shown in Figure 3. An unusual

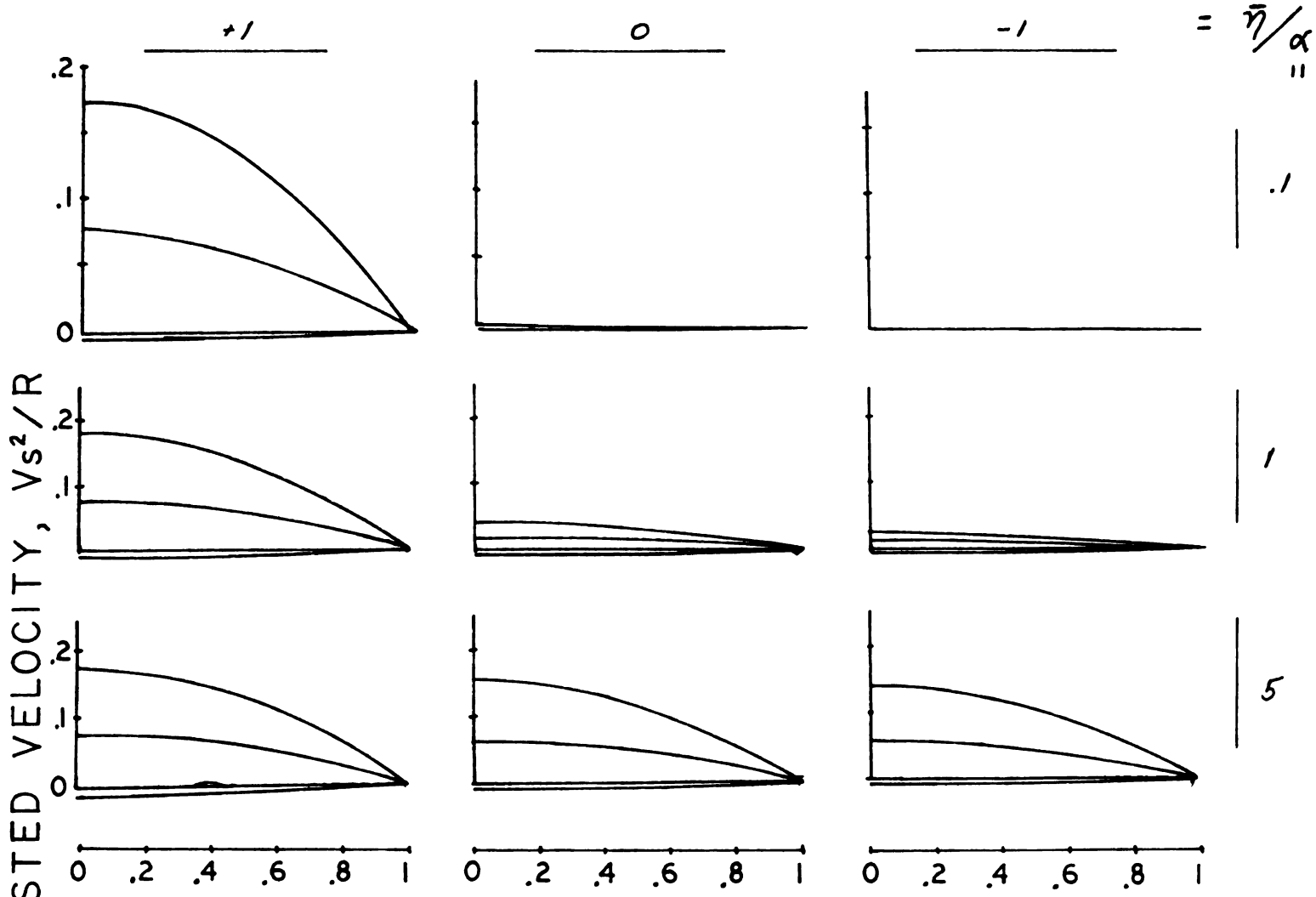

VELOCITY PROFILES ARE SHOWN FOR τ_w=.04, .2, .4 WHERE V INCREASES WITH τ_w.

FIGURE 3

VELOCITY PROFILE FOR THE FLUID WITH COUPLE & YIELD STRESSES

feature of the velocity profile is that, although the model contains a yield stress, the velocity extreme occurs at the center of the tube. This means that a plug flow region which exists in Bingham or Casson flow does not exist in this model, the limiting procedure using a plug region is invalid, and that it is valid to use Equation 7a for the entire tube cross-section.

Another important feature of Figure 3 is that negative flow rates are mathematically predicted for some low values of wall shear. Since negative flow rates are not physically possible for positive wall shear rates, this feature needs further investigation. Predicted negative flows are also a feature of Bingham or Casson flow uncorrected for the plug flow region. Since there is no plug flow region in this model, that cannot be used as an explanation here. The only realistic physical description at this point is that there is actually no flow while negative velocities are predicted and that flow begins only when positive velocities are predicted. That is, the velocity goes to zero everywhere as the wall shear stress approaches some lower limit, to be calculated next.

Since the velocity extreme predicted by Equation 7a occurs at the center of the tube, the predicted shear stress at which flow begins can be found by setting the velocity at r = 0 equal to zero. This gives

$$\tau_w/\tau_y = 1 - \pi/2\alpha \left[L_0(\alpha) + \frac{(1 - I_0(\alpha))\,(L_0(\alpha) - (1+\bar{\eta})L_1(\alpha)/\alpha)}{I_0(\alpha) - (1+\bar{\eta})\,I_1(\alpha)/\alpha} \right] \Big/ \left[1 + 2\,(1-\bar{\eta})(1 - I_0(\alpha))/(\alpha^2\,(I_0(\alpha) - (1+\bar{\eta})\,I_1(\alpha)/\alpha)) \right] \quad (9)$$

The only permissible values for α and $\bar{\eta}$ are those for which the right hand side of Equation 71 is unity, that is, the shear stress at which flow begins equals the yield value.

Figure 4 shows the ratio τ_w/τ_y predicted from Equation 9 for selected values of α and $\bar{\eta}$. Since all values are greater than unity, the yield stress obtained from static tests will never agree with the yield stress obtained from dynamic measurements. Therefore, this model will never be in agreement with the data obtained from whole blood.

The model can be forced into predicting a consistant yield stress by altering the boundary conditions stated by Valanis and Sun, Equation A 63 and A 64. Equation A 64 was invoked because A 63 was satisfied identically. Instead of Equation A 63, the second non-trivial boundary condition establishes a plug flow region at radii below the yield radius.

$$\partial v/\partial x = 0 \qquad \text{at } x = \tau_y/\tau_w \tag{10}$$

Since the flow rate is given by

$$Q = 2\pi R^2 \left[\int_0^{\tau_y/\tau_w} x\, v\, dx + \int'_{\tau_y/\tau_w} x\, v\, dx = \pi \left[v_y(\tau_y R/\tau_w)^2 + 2R^2 \int'_{\tau_y/\tau_w} v\, x\, dx \right. \right. \tag{11}$$

as x goes to one, the second term should go to zero as the range of integration goes to zero and the first term should go to zero as v_y approaches the velocity at the wall, which is zero. This should give a consistant value for τ_y.

Applying Equations A 62 and 11 to Equation A 61, the velocity is given by

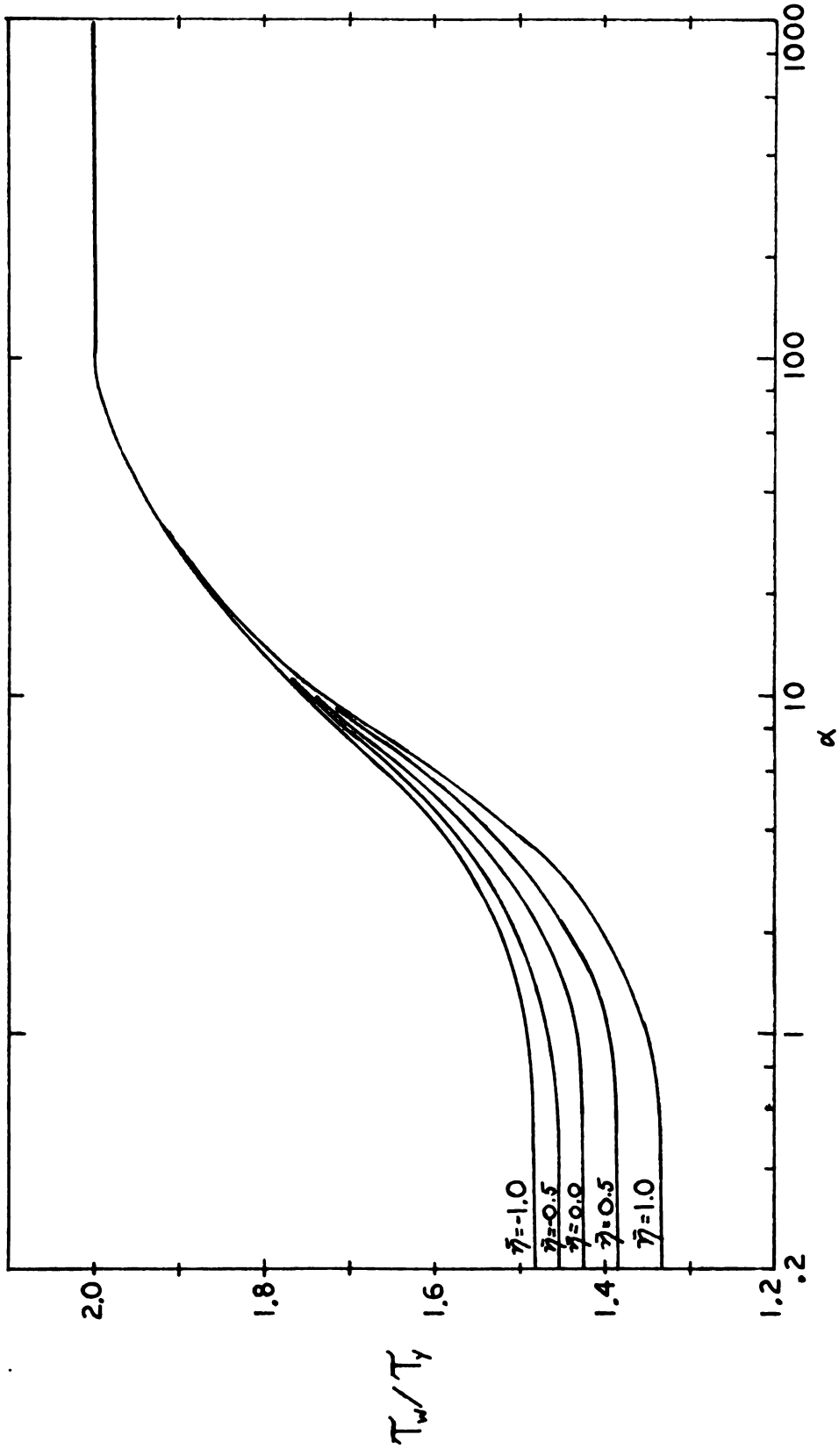

FIGURE 4
EXCESS SHEAR NEEDED FOR COUPLE STRESS MODEL

$$v = \tau_w R/2s^2 (1-x^2) - \tau_y R/s^2 \left[1-x- \pi/2\alpha (L_0(\alpha)-L_0(\alpha x)- (I_0(\alpha) - I_0(\alpha x)) (L_1(\alpha \tau_y/\tau_w) + 2/\pi\alpha^2)/I_1(\alpha \tau_y/\tau_w)) \right]$$

$$\text{for } \tau > \tau_y \qquad (12)$$

It can be immediately seen that the velocity does not go to zero as the wall shear stress approaches the yield stress and that, therefore, this approach will also not yield an equation applicable to the flow of whole blood. The process of the velocity everywhere going to zero cannot be used here since a plug flow region has been forced.

Another possible approach to the model is to force the gradient of vorticity to be zero at the centerline.

$$1/x \; d/dx(x \; dv/ \; dx) = 0 \qquad \text{at } x = 0 \qquad (13)$$

Then the velocity profile resulting from Equation A 62, A 63, and 13 is given by

$$v = \tau_w R/2s^2 \left[1 - x^2 - 4/\alpha^2 (I_0(\alpha) - I_0(\alpha x) \right] - \tau_y R/s^2 \left[1 - x - \pi/2\alpha (L_0(\alpha) - L_0(\alpha x)) \right] \qquad (14)$$

Again for the static and dynamic yield stresses to agree, either the velocity must go to zero for all x as τ_w approaches τ_y, which, it can be seen, is not the case, or the velocity gradient must go to zero at the yield radius, $r = \tau_y R/\tau_w$, and there be plug flow below this radius. If the derivative is formed, this is the case for

$$I_1 (\alpha \tau_y/\tau_w)/ L_1(\alpha \tau_y/\tau_w) = \pi/4(\alpha \tau_y/\tau_w) \qquad (15)$$

which is satisfied only if

$$\alpha \tau_y/\tau_w = 1.900 \qquad (16)$$

The "constant", α, is then a function of the shear stress at the wall and not a true constant. Therefore, this approach is also not valid.

No combination of realistic boundary conditions allows the concept of a couple stress in the form proposed by Valanis and Sun to describe the flow of blood. It was necessary to change their model by the inclusion of a yield stress in the description of the stress tensor because many investigators have demonstrated its existence. The yield stress must be simply additive so that the strain rate goes to zero as the stress approaches the yield value. However, if the yield stress is included in this form, the velocity profile then derived fails to exhibit features which have been observed in data using blood. Therefore, it must be concluded that these features are due to some phenomenon other than a couple stress.

THE FLUID WITH PARTICULATE TURBULENCE

Cinematographic studies of the flow of blood in cylindrical vessels [8,55] show that RBC's rotate and do not maintain a constant radial position. This movement of the particulate matter in whole blood precludes the establishment of a smooth velocity profile. Rather, the velocity distribution can more properly be described in terms of an average profile with a superimposed series of small, irregular fluctuations. Fluctuations superimposed on a steady velocity profile have long been noted in the turbulent flow of fluids and a branch of rheology called turbulence theory has grown to try to describe flow exhibiting these characteristics. The basic assumption of turbulence theory is that momentum is transferred during flow by two mechanisms. The first is laminar shear, the mechanism used in Newtonian flow. The second is the action of eddies or vortices. A vortex of diameter ℓ can transfer momentum by physically displacing some fluid (with a

momentum characteristic of its radial position) a distance ℓ to a new radial position (with a different characteristic momentum).

In Appendix A a model is derived which assumes that blood acts as a continuous laminar suspension of viscosity, μ, with eddies of rotating RBC's in it. The appropriateness of the assumption that a suspension can be described as a continuum in laminar flow is also discussed in Appendix A.

The equation which results for flow in a tube of radius R is (A 107)

$$Q/2\pi R^3 = \bar{U} = \Big[\tau_w/8 - \tau_y/6 + \tau_y^4/24\tau_w^3 + (\tau_w^2\,(b^5/80R^5 - b^2/48R^2 - b^4/48R^4 - b^3/48R^3) + \tau_y\tau_w\,(b^3/24R^3 + b^2/24R^2 + b/24R) - \tau_y^2\,(b^3/48R^3 + b^2/48R^2 + b/48R + 1/48) + \tau_y^5/120\tau_w^3)/\psi\mu + (\tau_w^3\,(-b^6/48R^6 + b^5/48R^5 + b^4/48R^4 + b^3/48R^3) + \tau_w^2\tau_y\,(3b^5/80R^5 - b^4/16R^4 - b^3/16R^3 - b^2/16R^2) + \tau_w\tau_y^2\,(b^3/16R^3 + b^2/16R^2 + b/16R) - \tau_y^3\,(b^3/48R^3 + b^2/48R^2 + b/48R + 1/48) + \tau_y^6/240\tau_w^3)/\psi^2\mu^2 + \ldots\Big]/\mu \qquad (17)$$

where Q is the volumetric flow rate, ψ is $\mu/2\rho H^2\ell^2\epsilon$, ρ is the fluid density, H is hematocrit, ϵ is a constant of proportionality ≤ 1, and b is the distance from the wall at which the laminar boundary layer begins.

Figure 5 shows Equation 17 for various values of μ and ψ. At high values of ψ, the model is indistinguishable from a Bingham model with equivalent yield stress and viscosity parameters. At a

FIGURE 5 COMPARISON OF CASSON AND TURBULENCE MODELS

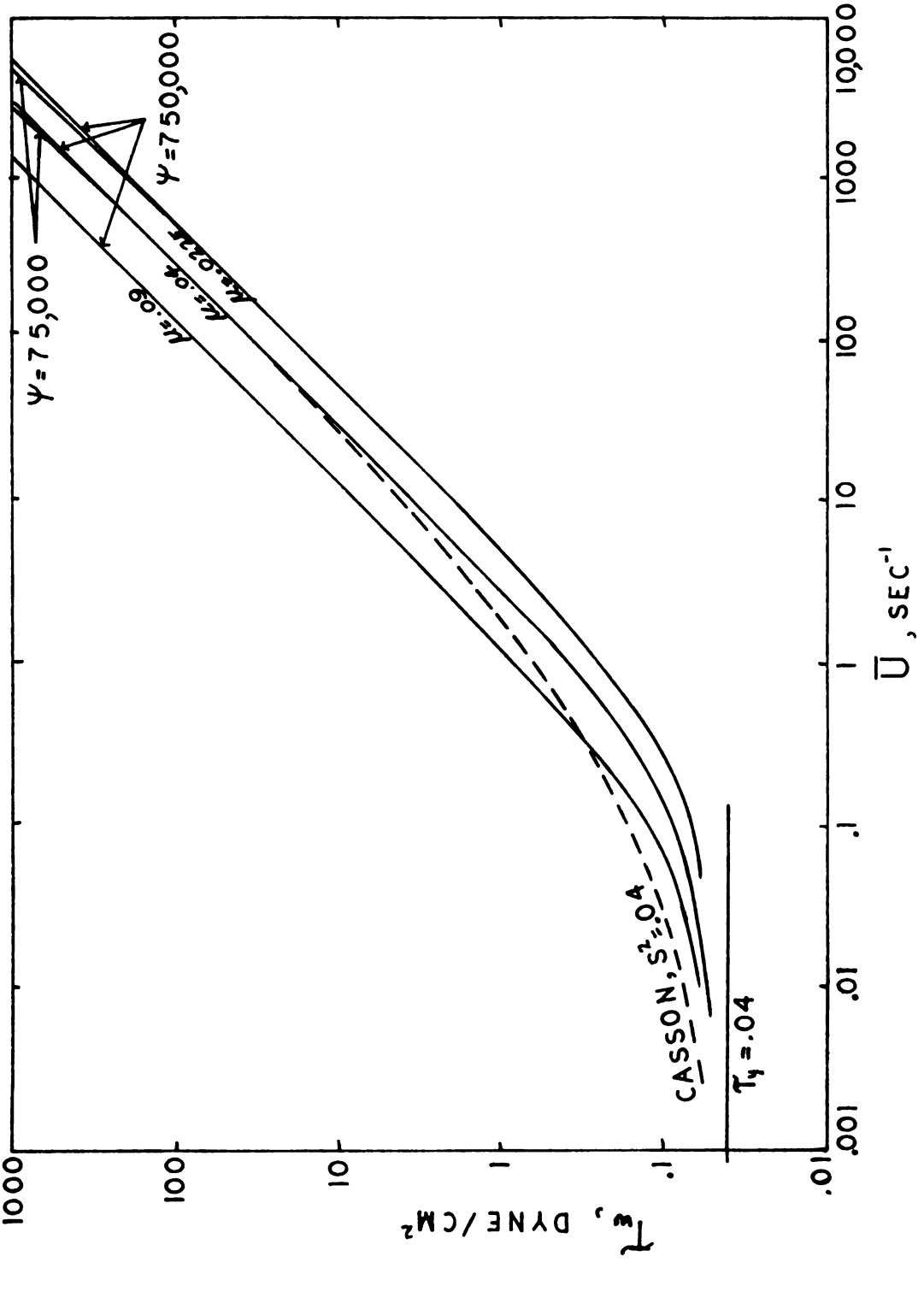

given value of wall shear stress, as φ decreases, the flow rate decreases. The magnitude of the decrease in flow rate grows as the value of the wall shear stress increases. At φ = 750,000 and τ_w = 1,000 the difference from the Bingham model is about 1%. This value of φ corresponds to individual RBC's rotating and a normal hematocrit. At φ = 75,000 and τ_w = 1,000, the decrease is about 8%. This value of φ corresponds to a grouping or rouleaux of three red blood cells. These results are for no marginal layer or b/R = 1.00. At b/R = 0.90, the discrepancy between the two models is decreased by approximately 25%. This value of b/R corresponds to a marginal layer one RBC wide in a tube 100μ in diameter.

Also shown in Figure 5 for comparison is the profile predicted by Casson's model, which is known to describe the flow of blood with only minor discrepancies. Identical yield stress values are used in both the Casson and turbulence models because the yield stress in a dynamic model must agree with the value obtained from an independent static test. This was discussed in the section on the couple stress model. The Casson model and turbulence model agree at wall shear stresses above 20 dynes/cm^2 only if identical viscosity coefficients are chosen for the two models. Then it is also necessary that the deviation due to turbulence be small so that the models agree at wall shear stresses above 300 dynes/cm^2. At wall shear stresses below 20 dynes/cm^2, the turbulence model and the Bingham model agree and both differ significantly from the Casson model.

This analysis of Figure 5 implies that momentum transport by the rotation of RBC's is negligible. In the range of wall shear

rates above 30 dynes/cm^2, momentum transport is indistinguishable from the amount predicted for a suspension of non-interacting particles. The linearity of the τ_w versus $\bar{U}$ plot in this region reflects the Newtonian nature of such a suspension.

Below 1 dyne/cm^2 significant non-linearity appears in the turbulence model. This is due to particle-particle adhesion due to the presence of a yield stress in the fluid. However, such a simple form of interparticle interaction does not describe the flow of blood for the Casson equation deviates from this model at wall shear rates below 30 dynes/cm^2. The flow rate for a given wall shear stress is always lower for the Casson model than for the model with the yield stress only. Therefore, the flow of blood must involve more complex interparticle interactions or other hydrodynamic features, such as doublet or larger size rouleaux formation. The inadequacy of the correlation of the square root of the shear rate with rouleaux size and concentration indicates that rouleaux formation is not the only important phenomenon. The shear rate induced orientation of RBC's is one possibility as is flushing of the cell biconcavity at higher shear rates. Both of these phenomena result in an altered hydrodynamic length-to-diameter ratio. Thus, the ability of Casson's equation to describe blood flow may rest with its ability to describe the combined effects of the hydrodynamics of flow around a single RBC and rouleaux formation rather than the effect of rouleaux formation alone.

Since it has been concluded that the Casson equation describes blood data better than any other model, it will be used to analyze the data collected in this study.

EXPERIMENTAL

EXPERIMENTAL

The two parameters in the Casson equation which can be determined experimentally are yield stress and high shear viscosity. An experimental apparatus and procedure was utilized which allowed a reliable extrapolation of these two parameters.

APPARATUS

The apparatus used to gather flow pressure data was designed after the apparatus used by Merrill et. al., [5] at Massachusetts Institute of Technology. The system, shown in Figure 6, uses a syringe drive to displace the experimental fluid from a sealed, constantly stirred reservoir through a precision bore capillary into another reservoir vented to the atmosphere. The pressure drop resulting from this forced flow is measured by a differential pressure transducer connected between both reservoirs.

A syringe drive (Model 940, Harvard Apparatus Company, Millis, Massachusetts) maintains a precise flow rate with a high torque, synchronous motor. An all gear, variable reduction drive train allows a series of twelve precise flow rates to be obtained. The syringes are also interchangeable to allow more flexibility in the variety of flow rates available. Most syringes used were Yale Multifit Tuberculin (Becton, Dickinson, and Company, Rutherford, New Jersey, or B & D) equipped with a Luer-Lok fitting although a 10λ syringe (Hamilton Company, Whittier, California) with Luer-Lok fitting attached with epoxy was also used for very low flow rates.

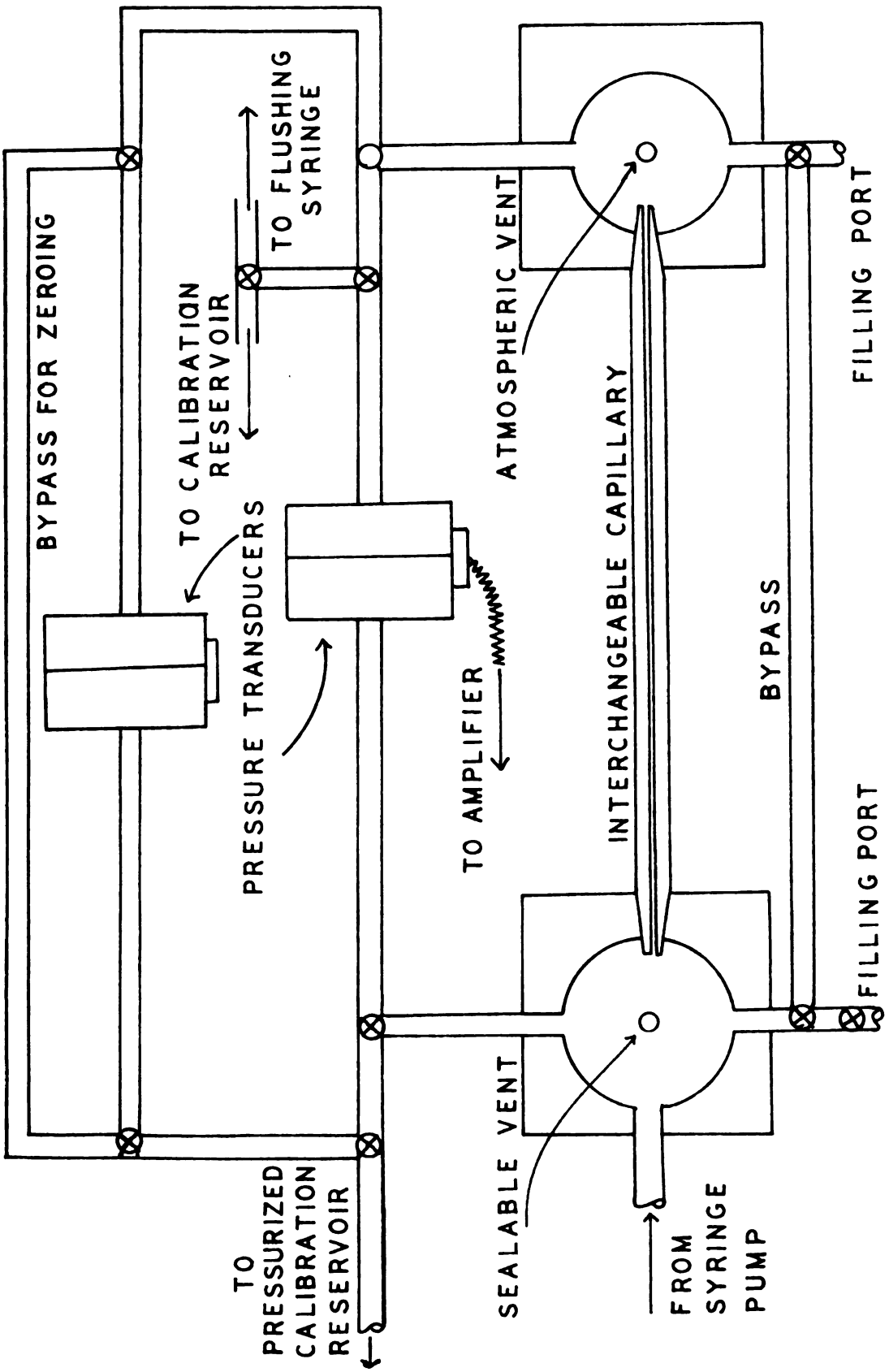

FIGURE 6 FLOW-PRESSURE APPARATUS DIAGRAM

The syringe is connected to the sealed reservoir with a 14 gauge stainless steel needle a Touhy-Borst adapter (B & D) and stainless steel Swagelok O seal adapter (Crawford Fitting Company, Solon, Ohio).

The upstream reservoir is a 3/4 inch diameter by 1½ inch cylinder machined from a two inch block of Plexiglas with a removable Plexiglas cover sealed by a one inch O ring. The cover is beveled towards the center vent to aid in the removal of bubbles. The vent is sealed with a silicone greased brass screw. The reservoir contents are stirred with a Teflon coated ball or rod rotated by a magnetic stirring motor located below the reservoir (See Figure 7). The air gap between the stirring motor and reservoir is flushed by an air stream to prevent heating of the experimental sample. In the block face opposite the syringe drive inlet is machined a one to ten or standard taper ($\overline{\$}$) for insertion of the interchangeable precision bore capillaries. In the other faces at the same height as the capillary port are Swagelok fittings for the bypass and the transducer circuit.

The capillaries were made from precision bore glass tubing (Fischer Porter Company, Warminster, Pennsylvania) and ground at both ends to standard taper. Some are shown in Figure 9.

The downstream reservoir is a 1 inch diameter by 2½ inch cylinder machined from a two inch block of Plexiglas with a removable Plexiglas cover sealed by a 1½ inch O ring. The cover is vented to the atmosphere through a two way valve (B & D). One face has a hole with a standard taper machined into it to accept the capillary.

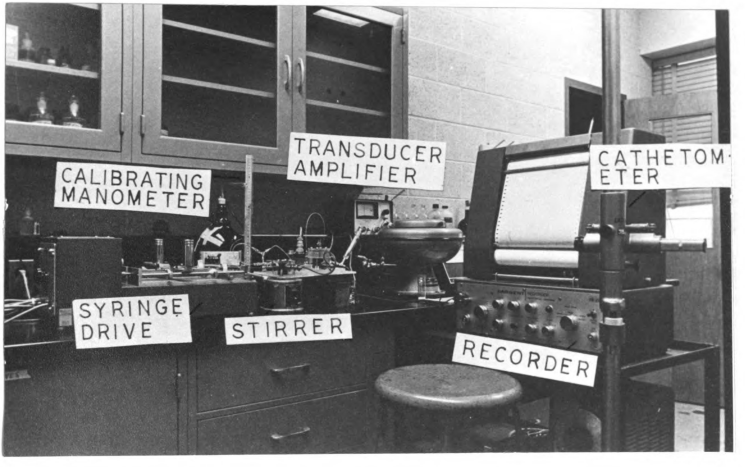

FIGURE 7 FLOW-PRESSURE APPARATUS USED

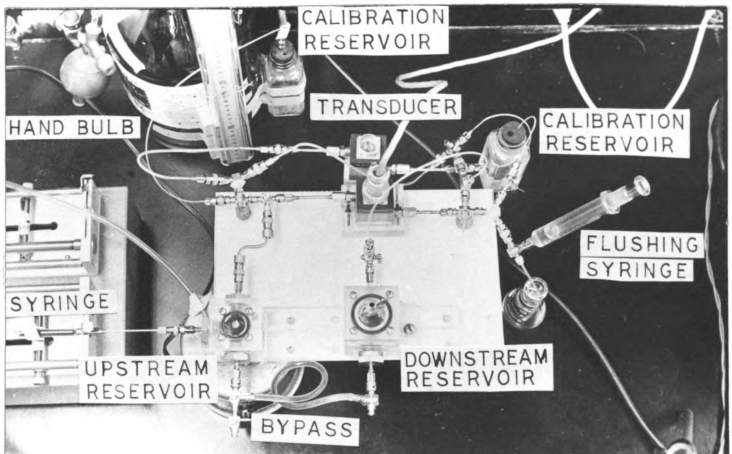

FIGURE 8 APPARATUS DETAIL

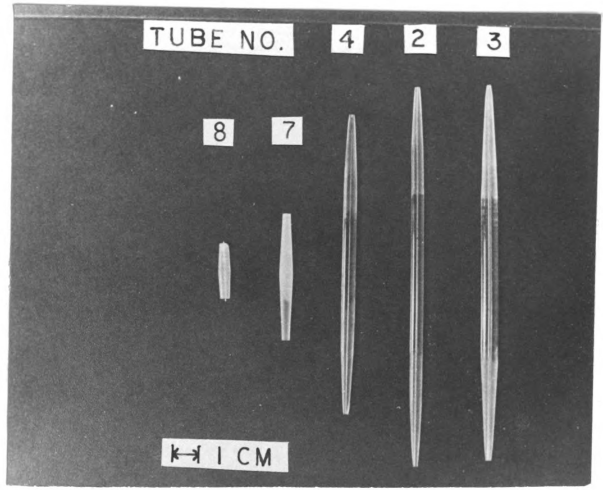

FIGURE 9 SOME PRECISION BORE CAPILLARIES USED

Adjacent faces are equipped with Swagelok adapters leading to the bypass and transducer circuit. While the sealed reservoir is attached to the Plexiglas base of the system, the downstream reservoir is movable in a track so various length capillaries can be fixed between the two reservoirs.

A section of one-eighth inch Tygon tubing is used as a bypass so the two reservoirs can be quickly brought to the same pressure. The bypass is also valved to allow filling of either reservoir with a syringe.

The transducer circuit is valved to permit either of two variables reluctance differential pressure transducers (Model KP15, Pace Engineering Company, North Hollywood, California) to be connected between the reservoirs or to the calibration system or to be zeroed. The transducer signal is amplified (Model CD 25, Pace) and recorded (Model MR, E. H. Sargent and Company, Chicago, Illinois). The calibration system consists of two reservoirs containing dialysate solution connected to the valving assembly by polyethylene surgical tubing, the end of which is immersed under the liquid level. While the downstream reservoir is always open to the atmosphere, the air space over the upstream reservoir can be pressurized by a hand bulb. The air space is also connected to one leg of a water manometer so the pressure can be determined. The level of the manometer legs are read with a cathetometer accurate to 0.005 cm. (Gaertner Scientific Company, Chicago, Illinois). The transducer circuit is also valved to allow any portion to be flushed with dialysate solution.

Hematocrits were determined after high speed centrifugation in heparinized capillary tubes (A. H. Thomas, Philadelphia,

Pennsylvania) and read on a special chart (Thomas). pH was determined on an expanded scale pH meter (Model 10, Corning Scientific Instruments, Corning, New York).

Several changes were made in the design of Merrill and co-workers. The entire system except the precision bore capillaries was constructed from plexiglas, polyethylene, and stainless steel since these materials do not induce clotting. This allowed lower levels of anticoagulent to be used. In addition, the feed reservoir was constantly stirred so change of hematocrit with time was minimized. The blood was not elaborately centrifuged to ensure uniformity of cells and thus was in a more natural state.

EQUIPMENT CALIBRATION

Transducer

The transducer was valved to the calibration system, the positive pressure side connected to the reservoir which may be pressurized and the negative pressure side connected to the atmospheric reservoir. One hour was allowed for the transducer amplifier to warm up. After this time, the manometer leg levels were read with the cathetometer to ensure there was no pressure in the upstream reservoir. The zero adjustment on the transducer amplifier was then turned until the same recorder reading was obtained on both the positive and negative polarity modes of the transducer amplifier. An offset from the edge of the recording paper was established with the displacement control on the recorder to facilitate this adjustment.

Then various pressure levels were established in the upstream reservoir by infusion or bleeding through the hand pump. Corresponding

manometer leg levels and recorder readings were recorded. Room temperature was monitored to ensure its constancy. The zero pressure reading was checked for constancy at the end of pressure series and its value subtracted from the other readings. The pressure was determined as $p = \rho gh$ where ρ is the density of water (the manometer fluid), g is the local value of the gravitational acceleration, and h is the difference in manometer leg levels. The almost linear correspondence between p and the recorder reading, r, is shown in Figure 10. Of the various simple algebraic expressions, the best correlation coefficient is obtained with

$$p = ar + br^2 \tag{18}$$

and this curve is shown in Figure 7 with best fit values for a and b.

It was observed that the best values of a and b did not remain constant if determined on different days, probably due to equipment drift. However, the ratio of the small non-linear coefficient to the linear coefficient did remain essentially constant. Therefore, during each day's experimentation, the transducer was calibrated at one pressure and recorder reading by

$$p = a(r + 0.0005462\ r^2) \tag{19}$$

Syringes

Each syringe to be calibrated was filled with clean mercury, fitted with a small bore needle, and mounted in the syringe drive assembly. Lines were scribed on the syringe drive screw and an adjacent stationary bracket. Infusion was started until mercury flowed from the needle tip and was stopped when the scribed lines became coincident. An empty beaker or watch glass was weighed to 0.0001 gm on a balance (Model EA-1AP, Torsion Balance Company, Clifton, New Jersey) then

FIGURE 10

PRESSURE TRANSDUCER RESPONSE

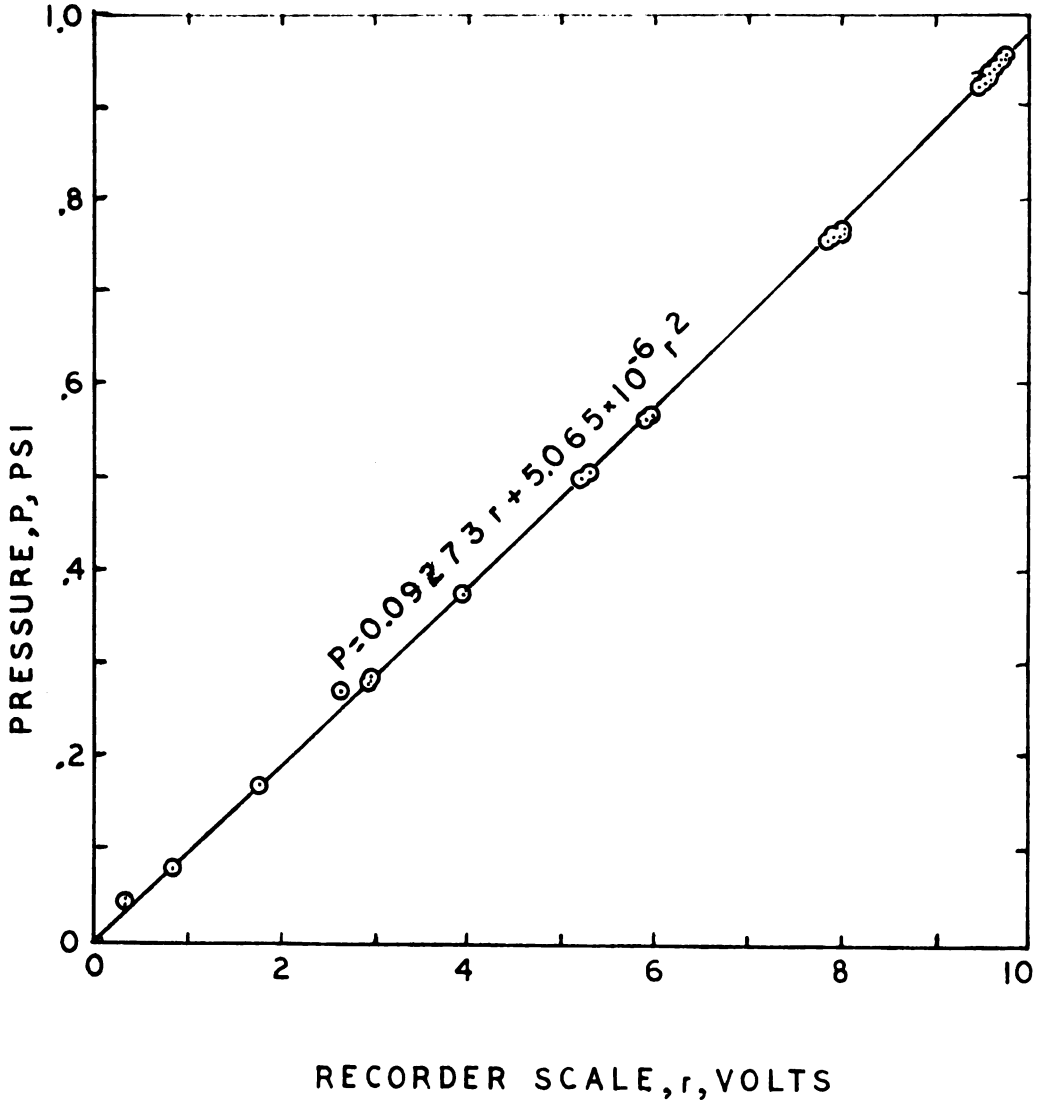

placed under the syringe needle. Mercury was forced into the beaker, in increments of screw revolutions and the increased weight of the beaker was recorded with the corresponding number of revolutions. Room temperature was monitored for constancy. Figure 11 shows the volume displacement with syringe drive screw revolution. The relation was assumed linear and the slope was determined and is shown on the figure.

Syringe Drive

The syringe drive screw rotation rate was checked by timing one hundred rotations at the highest rate with a laboratory timer accurate to 0.01 second. The scribe marks used for syringe calibration were the reference points. The rotation rate was 1 revolution per second with less than 0.1% variation whether or not the drive was loaded with a water filled syringe emptying through a small bore needle. The rotation rate at the next lowest rate was checked by timing fifty revolutions of the screw. Since the rotation rate was exactly one quarter the highest rate as anticipated from the rate table affixed to the syringe drive, and all rates were the result of direct gear drive, the lower rotation rates were derived by rate table ratio from the timed high rotation rate. The result of syringe drive and syringe calibration is shown in Table 2.

Capillary Tubes

The capillary tubes used were calibrated in the experimental apparatus. After the length of the tube to be calibrated was measured with a micrometer, it was mounted between the two reservoirs which were then filled with water. The stirrer was usually not used so that the recorder fluctuations due to its rotation would not be present and more

FIGURE II
SYRINGE CALIBRATION

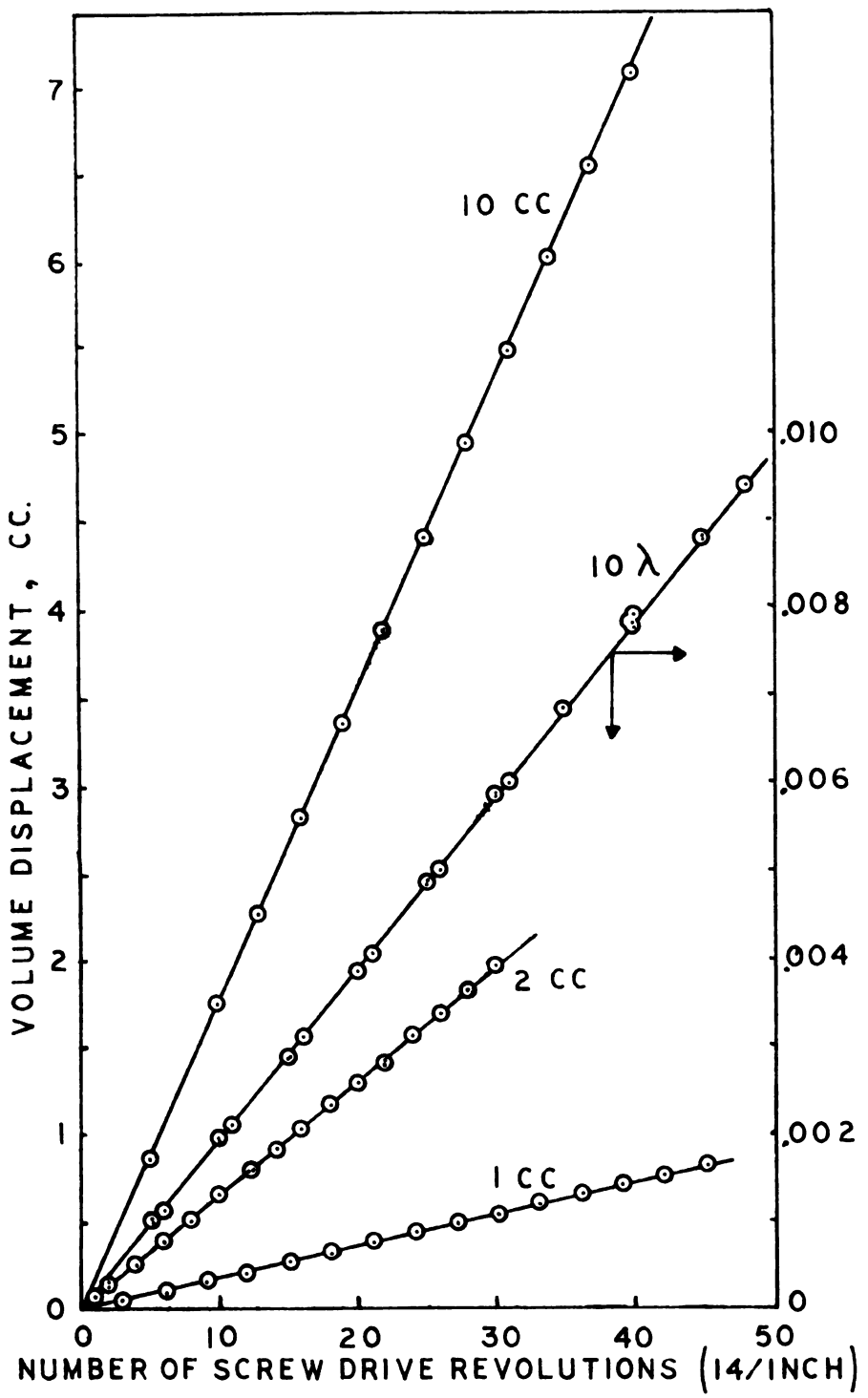

TABLE 2

FLOW RATES AVAILABLE

Gear Box Setting	Syringe 10 cc	2 cc	1 cc	10λ
1	10.70	3.96	1.11	.0119
2	4.28	1.585	.444	.00478
3	2.14	.793	.222	.00239
4	1.07	.396	.111	.00119
5	.535	.198	.0555	.000597
6	.214	.0793	.0222	.000239
7	.107	.0396	.0111	.000119
8	.0535	.0198	.00555	.0000597
9	.0214	.00793	.00222	.0000239
10	.0107	.00396	.00111	.0000119
11	.00535	.00198	.000555	.00000597
12	.00214	.000793	.000222	.00000239

Flow rates are in ml/min. The flow rates above represent the results of calibration calculations on the particular syringes used in this study and thus do not agree with the flow rate chart supplied with the syringe drive.

precise readings could be obtained. A series of pressure-flow points were obtained using the calibrated pressure transducer and syringe drive. The pressure drop was corrected for entrance and kinetic energy effects by subtracting 1.17 velocity heads according to the recommendations of Van Wazer, et al [67]. Since water is Newtonian and therefore obeys Poiseuille's Law and its viscosity is known as a function of temperature, all that is now unknown in Equation 1 is tube radius. This is calculated from the flow-pressure data. The results are shown in Table 3.

Other Equipment

The pH meter was calibrated daily with pH 7.00 buffer (Mallinckrodt Chemical, New York). In addition the span was checked once with pH 4.01, pH 7.00, and pH 10.00 and assumed constant.

The centrifuge head was fabricated by the Machine Shop of the Division of Engineering Research and thus needed standardization. This was accomplished by measuring its speed (6500 rpm) with a tachometer, calculating the time for centrifugation [29], and running duplicate blood samples at various hematocrits in a standard laboratory centrifuge (from the Department of Physiology) and in the fabricated centrifuge. Samples from twenty to seventy hematocrit agreed to within one unit.

EXPERIMENTAL PROCEDURE

For the ionic experiments, blood was drawn from dogs maintained by the Center for Laboratory Animal Resources at Michigan State especially as blood donors. The dogs were heparinized (5 mg/kg) to prevent blood coagulation and the blood sample was treated with additional heparin (½ cc 1% heparin/100 ml blood/day) if storage for a

TABLE 3

TUBE CALIBRATION RESULTS

Tube	Length CM	Number of Data Points	Temperature °C	Viscosity [35] cp	Diameter, μ Calculated	Average
1	16.048	24	28.20	.8298	502.6	503.5
		38	29.5	.8069	504.8	
		21	26.3	.8650	503.1	
		31	23.75	.9164	502.4	
		57	25.2	.8869	502.9	
2	15.796	24	28.5	.8244	396.8	397.8
		23	21.0	.9780	398.8	
3	15.659	40	23.15	.9296	986.2	986.2
4	12.464	8	29.4	.8086	165.7	164.8
		19	23.9	.9135	163.9	
5*	12.167	18	21.45	.9677	204.0	207.3
6*	10.371	24	22.8	.9373	207.3	207.3
7	5.220	15	24.2	.9073	128.5	128.1
		16	24.33	.9045	127.7	
9*	9.307	20	26.17	.8672	210.5	207.3
		23	26.64	.8587	207.4	

Note: * Tubes 5, 6, and 9 are the same tube ground to different lengths.

prolonged period was anticipated. Further treatment of the samples is described in the sections on the ionic effects and active hyperemia effects of the Results and Discussion chapter of this work.

Since the blood from the donors was usually obtained in a one liter polyethylene bottle, but the sample size for the rheometer was forty cubic centimeters, preparation of aliquots was the first step. The liter bottle was gently rolled to thoroughly mix the contents while preventing hemolysis from excessive shearing. The blood was then immediately poured into fifty cc. polyethylene bottles. These bottles were capped and refrigerated at 32°F. For the hyperemia experiments, samples were directly collected in the 50 cc. bottles.

Before using one of the aliquots, it was removed from the refrigerator and allowed to stand at room temperature for about forty-five minutes. When it was almost at room temperature, thirty-five cc. were poured into a glass beaker and five cc. of the desired isotonic diluent were added to the beaker. About fifteen minutes time was allowed for buffering and for transmembrane and thermal equilibrium to establish.

The pH meter was calibrated with buffered pH 7.00 solution and then the blood mixture pH was measured.

A 14 gauge stainless steel needle was attached to a syringe, the barrel of which was siliconized to prevent binding. The syringe was filled with the blood mixture and was then mounted on the syringe drive carriage and attached to the upstream reservoir. The syringe drive carriage was advanced until the fittings into the reservoir were filled. The drive was then turned on at the lowest speed so the syringe plunger would not bind.

The tapered ends of desired capillary were greased and mounted into the two reservoirs for a leakproof seal. The transducer circuit lines were flushed with dialysate solution and excess solution was removed from the reservoirs. The O rings on the reservoir covers were lightly siliconized and the covers were mounted and sealed. Agitation with the stirring ball and air gap cooling flow were started. The reservoirs were then filled. All bubbles were removed from the upstream reservoir which was then sealed with a siliconized brass bolt. The capillary was filled with blood so that meniscal effects would not affect the pressure drop results.

The pressure transducer was valved to the calibration reservoirs as in the calibration procedure for the transducer. The no pressure reading of the transducer was read on the recorder and the equal manometer leg heights were read by the cathetometer. The sealed reservoir was then pressurized with a hand bulb until the recorder reading almost went off the top of the chart. When the pressure reading became steady, the manometer leg levels were read by the cathetometer. The pressurized reservoir was then vented, and it was confirmed that the no pressure reading reestablished at the former level. Room temperature was recorded so the manometer fluid density would be known.

The pressure transducer valving was then turned so that the positive pressure tap connected to the upstream reservoir and the negative pressure tap connected to the vented reservoir. A pressure drop reading was then obtained for the lowest flow rate. The syringe drive was then stopped and a no flow reading obtained.

Next a flow rate was selected which gave a pressure reading of ten scale units or more. The syringe drive motor was started and the resulting pressure drop was recorded.

Then the flow rate was increased one gear stop and a new pressure reading was obtained. Progressively higher flow rates were selected until the pressure recorder reading exceeded chart capacity (ascending series). Then progressively lower flow rates were selected until the flow rate selected by the criterion cited in the previous paragraph was reached (descending series). The drive was then shut off and a new zero flow reading was obtained. Often this was not identical with and generally increased from the original zero flow reading. This change was found to occur when the pressure drop exceeded approximately 25 cm. of water. Thus, ascending pressures were compared with the original zero while descending pressures were compared with the final zero. When ascending and descending pressure drops were not similar at any flow rate, that flow rate was repeated and the inconsistent pressure drop was discarded.

The upstream reservoir sealing bolt was removed and the syringe drive carriage was advanced until the sealable vent was filled. Then a heparinized microhematocrit capillary tube was inserted into the reservoir until the lower end was at the same level as the precision bore capillary, and a sample was removed from this level. Hematocrits were determined in duplicate. Data for the sample was discarded if hemolysis was evident in the plasma portion of the tube after centrifugation.

The stirring motor and air gap flow were stopped. Blood was removed from the reservoirs by syringe and placed in a glass beaker. Blood pH was again determined and compared to the original value. Sets of data were discarded if the sample pH varied more than 0.1 pH from the control sample value.

The transducer circuit was flushed with dialysate solution. The rest of the apparatus was cleaned with water. In addition, the precision bore capillary was flushed with cleaning solution and then distilled water.

Blood pH, hematocrit, days since withdrawal, transducer calibration readings, room temperature, and flow-pressure data were entered on IBM cards for use by Fortran program TYNS (in Appendix B). Statistically best values for τ_y and s were obtained from a CDC 6500 computer by this program. The pressure drop correction used was 1.25 velocity heads recording to the recommendations of Van Wazer, et al [67] using the power law exponent of 1.22 derived by Hershey and Sung [33] for 35 hematocrit blood. The statistically best values for τ_y and s from both the experimental sample and its paired aliquot were then compared using a two-tailed Student's t-test. Significance of treatment effect (p value) and 95% confidence limits are reported on this basis. Because nonhomogeneous variance was noted in comparing the viscosity parameters (i.e. residuals increased with s), results are reported as % change from control viscosity to eliminate this defect.

RESULTS AND DISCUSSION

CATION EFFECTS

To study the effects of various individual cations, blood samples collected by the method described in the proceeding sections were mixed with isotonic (309 mOsm) solutions of sodium, potassium, magnesium and calcium chloride. A paired procedure was used whereby one aliquot of blood diluted with a chosen ionic solution was compared with another aliquot of the same blood diluted with dialysate solution. Five cubic centimeters of the above solutions were combined with thirty-five cubic centimeters aliquots of whole canine blood prior to viscosity determination. A constant 1:7 dilution was chosen so that hematocrit variation between samples was minimized and so that the hematocrit level was near normal. Isotonic solutions were used so that tonicity effects were eliminated as a source of error.

This procedure markedly increases the concentration of the cation studied, but to a lesser degree, the concentrations of the other ions are also affected. For example, dilution with isotonic calcium chloride raises the calcium ion level from 5.0 meq/l to 17.3 meq/l. However, the concentration of the other cations are reduced. Magnesium falls from 2.0 meq/l to 1.8 meq/l, sodium level is reduced from 140 meq/l to 122 meq/l, potassium from 4.35 meq/l to 3.81 meq/l. Chloride concentration is increased from 102.5 meq/l to 109.0 meq/l. Bicarbonate decreases from 24.6 meq/l to 21.5, phosphate from 1.2 meq/l to 1.1 meq/l. Changes resulting from this treatment may be ascribed to the calcium ion change alone if the Casson viscosity and yield stress do not vary significantly with the concentration of the other ions. It will be seen that this is the case.

This dilution treatment yields only one ion concentration higher than the control value. The low ionic concentration was achieved by using saline as diluent. Since it was desired to collect data relevant to the different resistance results which have been noted for mild and severe hyperkalemia, an alteration of the standard procedure was used to produce these conditions. If isotonic solutions of potassium chloride and sodium chloride are mixed in various ratios, any concentration of potassium ion is possible from zero to the isotonic value. A mixture was used which gave potassium ion concentration of one-half the maximum. Thus, counting the standard solutions, potassium was available as none, half, or all of the added cation concentration. Three runs were made with potassium as one quarter of the added cation but, due to the small sample size, the results from these runs are not analyzed here.

Data were collected in the flow-pressure apparatus previously described and analyzed by computer program TYNS (listed in Appendix B) for viscosity and yield stress. The results of these calculations are listed in Table 4 in Appendix C. A summary of the average effects is given in Table 6. The tube diameter used most for these runs was 200μ.

Figure 12 shows the effects of cation concentration on the viscosity parameter of the Casson equation. This is the viscosity at a high shear rate. One to seven dilution of blood with isotonic potassium chloride produces blood with 22.6 meq K^+/l, if it is assumed that the undiluted blood contains the normal average of 4.4 meq K^+/l. Actual blood potassium level should not be far from the normal, since

FIGURE 12

CATION EFFECT ON CASSON VISCOSITY

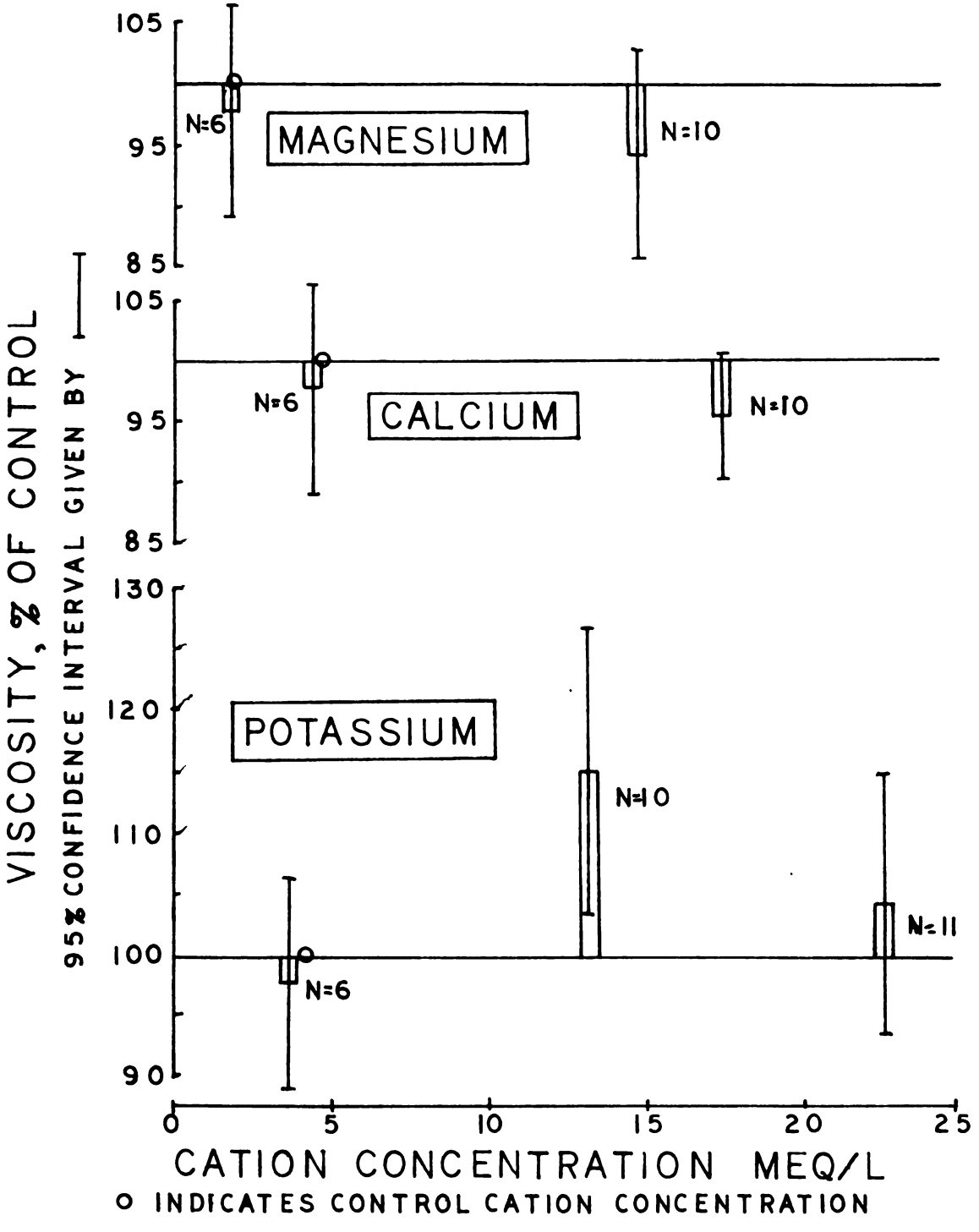

blood was collected from dogs maintained by the Michigan State University Center for Laboratory Animal Resources especially as blood donors. Average blood viscosity at this potassium level is elevated 4.1% over the corresponding control, which is another aliquot diluted with dialysate solution. The increase is not significant at the .05 level. Blood viscosity is elevated 15.2% above control at a potassium ion concentration of 13.2 meq/l. This is significant at the 0.01 level. Dilution of blood with saline results in a 2.1% decrease in viscosity, which is not significant at the .05 level. This corresponds to a potassium ion concentration of 3.9 meq/l.

Elevation of blood calcium level from 4.7 meq/l to 17.3 meq/l results in a 4.5% decrease in viscosity. This is not significant at the 0.05 level. Elevation of blood magnesium from 2.0 meq/l to 14.7 meq/l results in a 5.0% decrease which is not significant at the 0.05 level.

Figure 13 shows the effect of various cation concentrations on the yield stress. None of the changes are statistically significant.

The lack of any significant change of viscosity or yield stress with dilution by saline or magnesium chloride suggests that the slight increase in chloride ion concentration or decrease in any other anion concentration accompanying these dilutions also have no effect on either the Casson viscosity or yield stress over the range which the anions varied. Otherwise, any change due to anion concentration would have to be counterbalanced exactly by the effects of each of these cations, and this would be highly unlikely.

FIGURE 13

CATION EFFECT ON YIELD STRESS

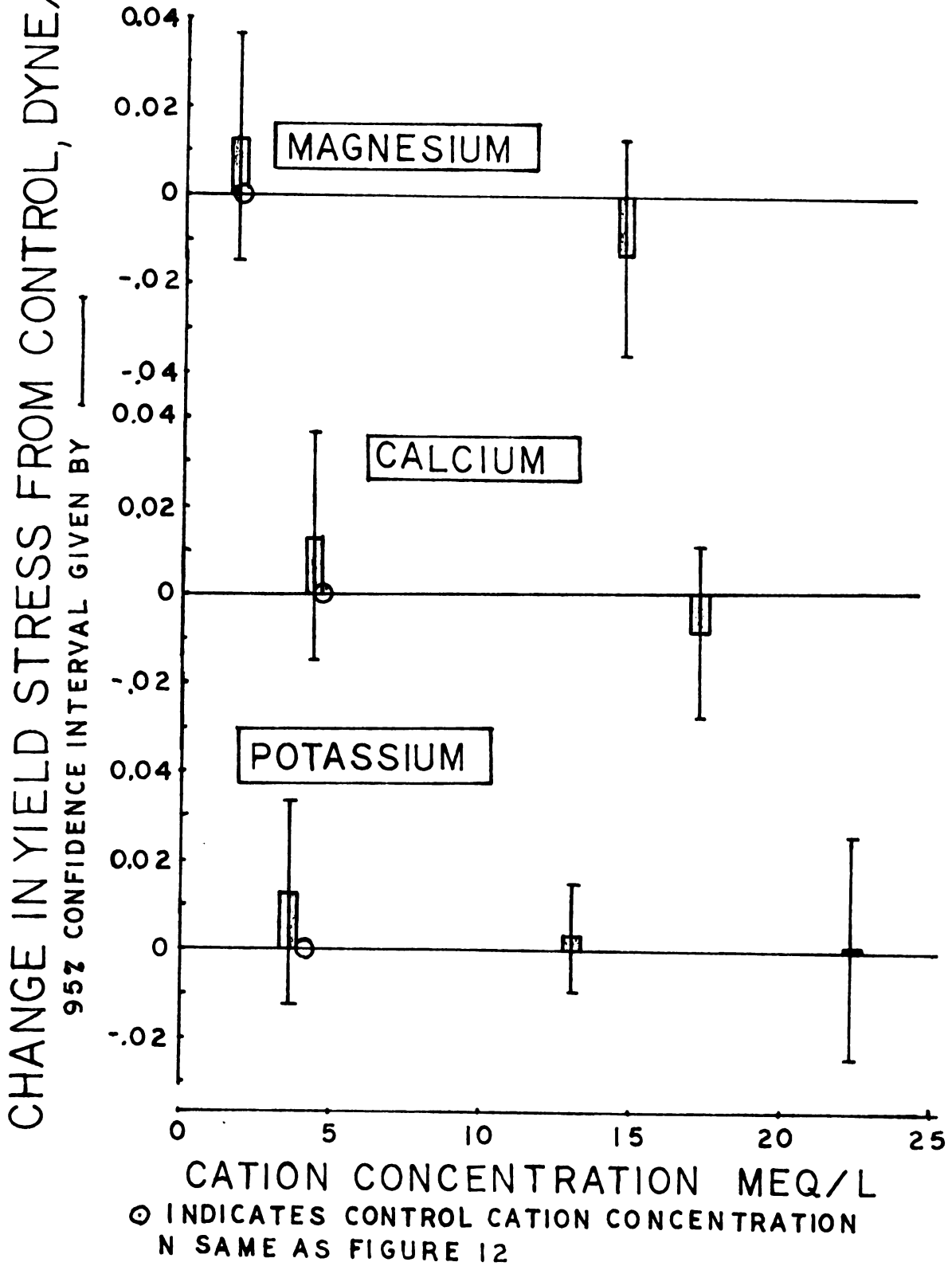

⊙ INDICATES CONTROL CATION CONCENTRATION

N SAME AS FIGURE 12

pH EFFECTS

To study in a viscometer the effect of pH on the Casson flow parameters, it is necessary to increase and decrease the pH of some aliquots from the normal value. There are three possible methods to do this. Two are aeration with varying mixtures of oxygen and carbon dioxide and admixture with isotonic solutions of differing pH. The results from these two procedures are complicated by the effect of pH on hematocrit [48, 50] and the resulting effect of hematocrit on the Casson parameters. Decreasing pH is associated with swelling of RBC's because of the water movement accompanying bicarbonate ion diffusion, and a resulting increased hematocrit. The third method of adjusting pH is admixture with non-isotonic solutions of differing pH. If the tonicity of these solutions are properly adjusted, RBC size and therefore hematocrit will not change. Since it is not the purpose of this study to determine the effects of altered tonicity, and since altered hematocrit is the natural response of whole blood to pH change, admixture with isotonic solutions is used here.

Control procedure for this series of experiments consisted of admixture of 35 cc. of whole blood with 5 cc. of dialysate solution as in the ionic section. The yield stress and viscosity of the collected data are listed in Table 4 of Appendix C and are summarized in Table 6. Average hematocrit of eleven control samples was 33.94. Average pH of controls was 7.428 for comparison with low pH treatment and was 7.444 for comparison with high pH treatment. Average yield stress of controls was 0.0306 dyne/cm^2 for comparison with low pH treatment and was 0.0273 for comparison with high pH treatment. The tube diameter used was 400μ.

Low pH was attained by admixtures of blood with a 1:1 mixture of isotonic HCl and dialysate solution. This mixture was used because pure isotonic HCl gave values of pH far outside natural limits. Dilution was the same as with control so that there was no viscosity change due to different protein levels [40]. Average blood pH was 7.024. Average hematocrit was 37.10. Blood viscosity increased 1.41%, but this change is not significant at the .05 level. Average yield stress increased by 0.019 dyne/cm^2, and this change is significant at the 0.01 level.

High pH was attained by admixture of blood with a 1:3 mixture of isotonic NaOH and dialysate solution. Dilution was the same as with control. Average blood pH was 7.831. Average hematocrit was 32.27. Average blood viscosity increased 0.53%, but this change is not significant at the .05 level. The average yield stress fell by 0.0042 dyne/cm^2, but this change is not significant at the .05 level.

The observed increase in yield stress at decreased pH might be attributed to pH induced swelling. However, since the viscosity does not increase, this hypothesis must be considered suspect. Since RBC's are positively charged particles, it is possible that a change in pH toward making their environment more positively charged (more H+ or lower pH) would enhance their self-attraction, and thus result in an increased yield stress.

ACTIVE HYPEREMIA

A natural process during which ionic and pH changes occur is exercise or active hyperemia. For example, hydrogen and potassium ion concentrations increase during exercise [57]. It is desired to determine if the altered resistance to flow observed during active hyperemia can be explained by viscosity changes due to ionic effects.

The organ used in this study was the canine gracilis muscle. Preparation involved anesthetizing the dog with sodium pentobarbitol (30 mg/kg) and ventilating with a mechanical respirator. The right gracilis was surgically exposed and freed from connective tissue. All blood vessels connected to the muscle except the major artery and vein were ligated. Heavy occlusive cord ligatures were placed at each end of the muscle to completely eliminate collateral flow. A short section of the gracilis nerve was freed from investing fascia and encircled with a loose ligature. The gracilis vein was cannulated and its outflow diverted to a polyethylene collection bottle. Sodium heparin (5 mg/kg) was injected intravenously to prevent coagulation.

In small dogs, the leg vein was cannulated instead of the gracilis vein so a larger cannula could be used. Lower back pressure results and thus the transcapillary pressure rise accompanying increased flow was minimized.

A sample was taken under natural flow conditions. This was used as control. Electrical stimulation was then applied to the gracilis nerve (6-10 volts, 0.06 msec duration, 6/sec frequency). After several minutes, venous outflow was collected as the active hyperemia sample. Most samples were collected in the late morning, refrigerated, and run within four hours. Several runs were collected from the cannula under

mineral oil to minimize gaseous exchange with the atmosphere. These samples are designated in the Appendix. The most frequently used tube diameter was 400μ.

During active hyperemia, blood hematocrit increased to an average of 44.33 from the control average of 41.27. A viscosity increase of 12% is predicted from viscosity versus hematocrit charts for this change. Despite this predicted increase, the Casson viscosity as determined in the experimental apparatus did not change. A statistically insignificant decrease of 3.3% was observed. Average pH changed from 7.384 to 7.249 during active hyperemia, and the pH results from the previous section imply no effect on viscosity. Blood potassium increases during active hyperemia,but this also may result in an increased viscosity depending on the potassium level attained. While it has long been known that vasoactive agents are released during active hyperemia, the fact that the observed lack of viscosity change cannot be explained on the basis of altered hematocrit, pH, and ionic concentrations suggests thatviscoactive agents may also be released, or the results may be due to some other ionic effect not investigated.

Although the observed lack of change in viscosity cannot be explained in terms of the variables studied, the lack of increase in resistance to flow expected from pH and hematocrit changes is fortunate since increased blood flow is needed to supply oxygen and to remove metabolic by-products from exercising muscle.

An increase in the yield stress by 0.028 dyne/cm^2 from an average of 0.0374 dyne/cm^2 was also observed. This is statistically significant at the 0.01 level. Decrease in pH is associated with a marked increase in yield stress so most of this increase could be due

to a pH effect. Increase in blood potassium has no effect on yield stress. Also, yield stress is roughly proportional to the hematocrit cubed [44], so an increase in Hct also implies an increased yield stress. Another factor is pertinent here since this is an in vivo experiment.

Siegel and Kolmen [58] have found that during metabolic or respiratory acidosis, the fibrinogen level in plasma or lymph is inversely proportional to pH. Thus, decreased pH should yield elevated fibrinogen levels. Merrill, et al., [43, 46] and Walder, Weaver, and Evans [67] have found that yield stress is proportional to fibrinogen concentration. Therefore, an increase in yield stress should result from the pH induced increase in fibrinogen.

Thus, the increase in yield stress may be explained as the sum of effects of pH, hematocrit, and fibrinogen.

SUMMARY

Two rheological models were investigated - a couple and yield stress model and a turbulence model.

The couple stress model proposed by Valanis and Sun fits some blood velocity profiles well, but the model lacks a yield stress. Since a yield stress has been demonstrated by many investigators in blood, one must be included in any model which is to describe blood flow. If this is done, negative velocities are predicted for some wall shear rates above the yield value using a variety of boundary conditions. Since this is physically impossible, the concept of a couple stress does not truly describe blood rheology.

If turbulence theory is applied to the flow of blood, it is concluded that momentum transport by the eddy-like rotation of RBC's is negligible when compared to momentum transport by laminar flow of a suspension of RBC's in plasma. At low shear rates, there are more particle-particle interactions than proposed by a simple yield stress fluid.

The best available rheological model for blood flow is the Casson model. It was used to investigate the effects of altered cation concentration and of active hyperemia.

The concentration of the principal cations (sodium, potassium, calcium, magnesium, and hydrogen) in canine blood was altered by 1:7 dilution with isotonic salt solutions differing in their

ionic makeup. Blood viscosity increased 15.2% at a potassium ion concentration of 13.2 meq/l when compared with control blood (4.2 meq K^+/l). Control blood was a paired aliquot of blood diluted 1:7 with dialysate solution to maintain tonicity, hematocrit, and other ionic concentrations at the same level as the test sample. This viscosity increase is significant at the 0.05 level. Low pH (7.02) blood had a 0.019 dyne/cm^2 higher yield stress than control blood (pH 7.43) with a significance of less than 0.01. Other cation concentration levels produced no significant changes.

Venous outflow from a canine gracilis during active hyperemia was not different in viscosity from the venous outflow prior to stimulation. However, the yield stress was an average of 0.028 dyne/cm^2 higher, which change is significant at the 0.01 level.

RECOMMENDATIONS

To improve the accuracy and utility of the experimental apparatus used here, several modifications might be made. Periodic variations in the pressure drop readings have been noticed, and the period decreases with increasing flow rates. This might be due to imperfections or non-uniformity in the drive screw or to gear lash in the drive train. These defects can be corrected by regrooving the drive screw and movable carriage and by changing the drive train to square tooth gears. The latter modification will, of course, make it more difficult to change speeds. However, the pressure drop readings will then be more precise due to a more uniform flow rate supply. There are also fluctuations in the pressure reading due to the physical impact of the stirring ball on the reservoir walls. These could be eliminated by allowing the ball to rotate on a pin or by making a dishshaped floor in the reservoir so that the ball would not climb up and come in contact with the walls. The brass seats on the B&D valves wear out rather rapidly and the valves could be replaced by a more durable type to eliminate this problem.

This study has found an elevated yield stress in blood of low pH and in blood from active hyperemia. An elevated level of fibrinogen has been implicated as the causative mechanism. The concentration of fibrinogen in active hyperemia blood should be determined to confirm this hypothesis.

APPENDICES

APPENDIX A

APPENDIX A

MATHEMATICAL DERIVATIONS

1. Poiseuille Flow of a Casson Fluid

For steady state axial flow of a fluid in a tube, the Navier - Stokes equation reduces to

$$dp/dz + 1/r\ d/dr\ (r\ \tau) = 0 \qquad \text{(A 1)}$$

Since the first term is a function of z only, it is constant. Let $dp/dz = -\Delta p/L$ where L is the length of the tube considered. If Equation A 1 is multiplied by r and integrated

$$+ (\Delta p/2L)\ r^2 + r\ \tau = C_1 \qquad \text{(A 2)}$$

From symmetry τ is zero at the centerline. Equation A 2 thus requires that C_1 be zero at r = 0. Thus

$$\tau = -\Delta p\ r/2L \qquad \text{(A 3)}$$

Equation 2 on page 9 can be rearranged to give

$$s(-dv/dr)^{1/2} = \tau^{1/2} - \tau_y^{1/2} \qquad \text{(A 4)}$$

Combining Equations A 3 and A 4, and squaring,

$$-dv/dr = \left[-\Delta p\ r/2L - (-\Delta p\ r2\tau_y/L)^{1/2} + \tau_y\right]/s^2 \qquad \text{(A 5)}$$

Integrating with respect to r

$$-v = \left[-\Delta p\ r^2/4L - 2/3\ (-2\Delta p\ \tau_y/L)^{1/2}\ r^{3/2} + \tau_y r\right]/s^2 + C_2 \qquad \text{(A 6)}$$

From the lack of slip at the wall, v = 0 at r = R.

$$0 = \left[-\Delta p\ R^2/4L - (-8\Delta p\ \tau_y/9L)^{1/2}\ R^{3/2} + \tau_y R\right]/s^2 + C_2 \qquad \text{(A 7)}$$

Equations A 6 and A 7 imply the velocity profile is

$$v = \left[(-\Delta p/4L)(R^2-r^2) - \sqrt{-8\Delta p\ \tau_y/9L}\ (R^{3/2} - r^{3/2}) + \tau_y(R-r)\right]/s^2 \qquad \text{(A 8)}$$

Recall that the Casson model is valid only for shear stress greater than the yield value. Since the shear stress is linear with radius in Poiseuille flow, Equation A 8 is valid only radii greater than the radius, r_y, at which the shear stress reaches the yield stress.

The flow rate of a Casson fluid can be obtained by integrating the velocity across the tube.

$$Q = 2\pi \int_0^R vrdr = 2\pi v_y \int_0^{r_y} rdr + 2\pi \int_{r_y}^R vrdr \qquad \text{(A 9)}$$

where v_y denotes the constant velocity at radii at or below r_y.

$$Q = \frac{\pi r_y^2}{s^2}\left[\frac{-\Delta P}{4L}(R^2-r_y^2) - \sqrt{\frac{-8\Delta P \tau_y}{9L}}(R^{3/2}-r_y^{3/2}) + \tau_y(R-r_y)\right] \qquad \text{(A 10)}$$

$$+ \frac{2\pi}{s^2}\int_{r_y}^R\left[\frac{-\Delta P}{4L}(R^2r-r^3) - \sqrt{\frac{-8\Delta P \tau_y}{9L}}(R^{3/2}r-r^{5/2}) + \tau_y(Rr-r^2)\right] dr$$

From Equation A 4, the shear stress at the wall, τ_w, is given as $-\Delta pD/4L$. Also from Equation A 4 may be obtained the expression for the yield radius.

$$r_y = \tau_y R/\tau_w \qquad \text{(A 11)}$$

If Equation A 11 is substituted into the integrated Equation A 10, like terms in powers of τ_w can be collected to give

$$Q = \pi D^3\left[\tau_w/4 - 4\sqrt{\tau_y\tau_w}/7 - \tau_y^4/84\tau_w^3 + \tau_y/3\right]/8s^2 \qquad \text{(A 12)}$$

Expressing the average velocity in tube diameter per time,

$$\bar{U} = \frac{4Q}{\pi D^3} = \left[\tau_w/4 - 4\sqrt{\tau_y\tau_w}/7 - \tau_y^4/84\tau_w^3 + \tau_y/3\right]/2s^2 \qquad \text{(A 13)}$$

is the desired expression for Poiseuille flow of a Casson fluid.

2. Poiseuille Flow of a Fluid with Couple and Yield Stresses

To solve the problem of Poiseuille flow of a fluid with both couple and yield stresses, the appropriate differential equations must first be derived from the principles of continuum mechanics.

Figure 14 shows a fluid element in a velocity field and the forces acting upon it. Forces acting to change the linear momentum of the element are the two traction forces, pressure and shear. By the definition of a couple as two equal forces acting in opposite directions, but separated by a lever arm, the net effect of a couple upon the linear momentum of the element is zero.

Forces acting to change the angular momentum of the element are the couple stress and the shear stress. Since the pressure stress acts only perpendicularly to the faces of the element, the net effect of the pressure upon the angular momentum of the element is zero.

The first equation of motion can be obtained by considering the linear momentum of the fluid element. At any point in time, t, the linear momentum in the ith coordinate direction, P_i, of all particles in the domain, D, is

$$P_i = \int_D \rho v_i dV \qquad \text{(A 14)}$$

where ρ is the fluid density, and v_i is the instantaneous velocity in the ith coordinate direction. If the domain is subjected to surface tractions, T_i, the resultant force, F_i, on the body is

$$F_i = \oint T_i dS \qquad \text{(A 15)}$$

where dS is a surface element of D. If the tractions are decomposed by Cauchy's formula [24] into components

$$T_i = \tau_{ji} n_j \qquad \text{(A 16)}$$

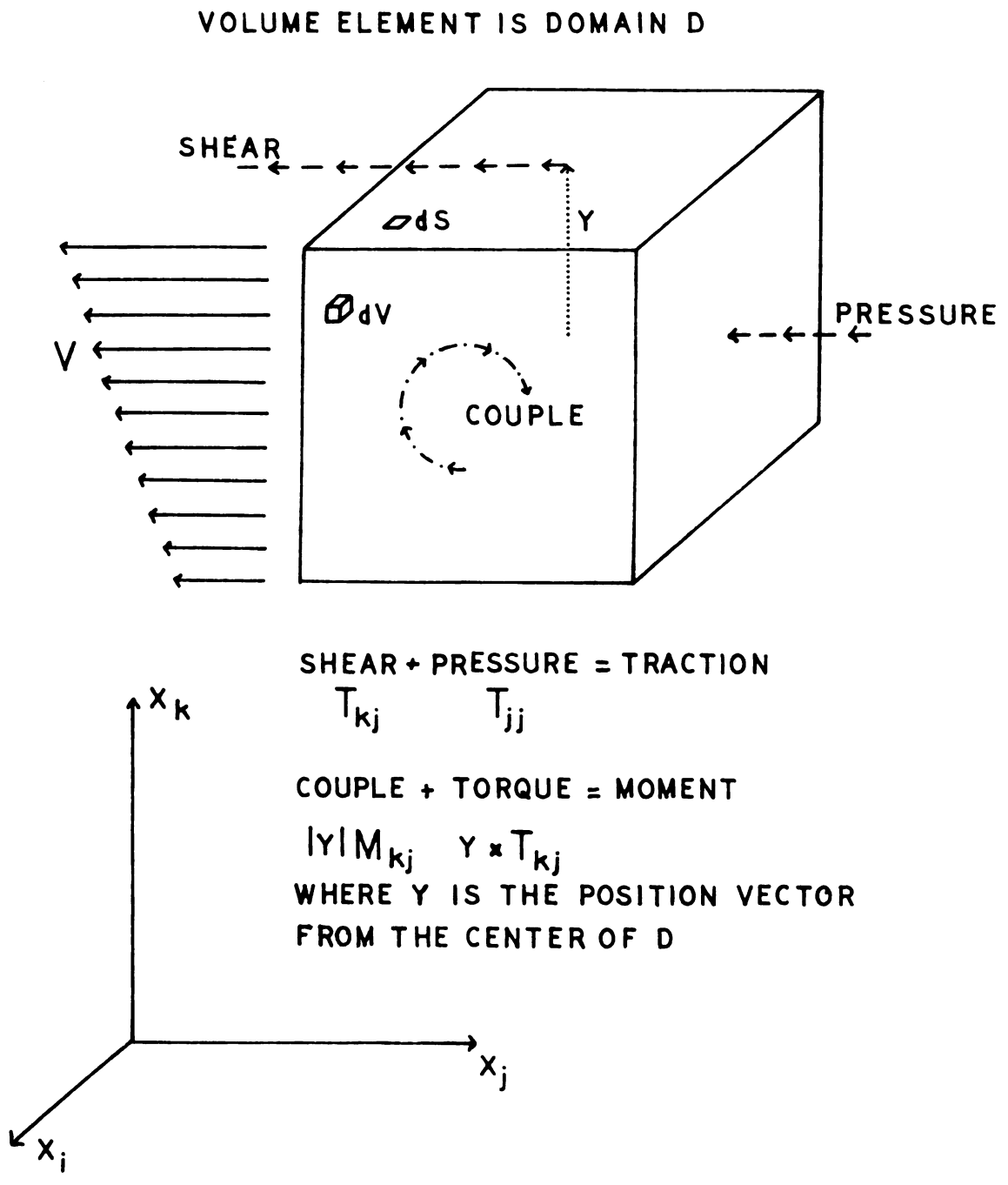

FIGURE 14

FORCES ACTING ON A FLUID ELEMENT

where n_j is an orthonormal vector directed outward in the jth coordinate direction, Equation A 15 can be transformed by the Green-Gauss theorem [25] into the volume integral

$$F_i = \int_D \partial \tau_{ji} / \partial x_j \, dV \qquad \text{(A 17)}$$

Newton's Second Law states that the rate of change of linear momentum of a body is equal to the force acting on that body. This can be expressed in the Eulerian reference system as

$$\frac{D}{Dt} P_i = F_i \qquad \text{(A 18)}$$

Combining Equations A 14, A 17, and A 18.

$$\frac{D}{Dt} \int_D \rho v_i \, dV = \int_D \partial \tau_{ji} / \partial x_j \, dV \qquad \text{(A 19)}$$

Since Equation A 19 is true for any choice of domain, the kernels of the integrals must be equal

$$\rho \, Dv_i/Dt = \partial \tau_{ji} / \partial x_j \qquad \text{(A 20)}$$

This is the first equation of motion or Cauchy's First Law. [7]

When considering angular momentum it is customary to use the vorticity vector, w_i, which is defined [60] as half the curl of the velocity vector, instead of the velocity vector,

$$w_i = 1/2 e_{ilm} W_{lm} = 1/4 e_{ilm} (\partial v_m / \partial x_l - \partial v_l / \partial x_m) \qquad \text{(A 21)}$$

where e_{ilm} is the cyclic permutation number [26], or the permutation tensor, and W_{ij} is the vorticity tensor. Considering the angular momentum instead of the linear momentum the equivalent of Equation A 19 is

$$\frac{D}{Dt} \int_D |Y| \rho w_i dV = \int_D (|Y| \partial \mu_{ji} / \partial x_j + Y \times \tau_{ji}) \, dV \qquad \text{(A 22)}$$

where μ_{ij} is the couple stress tensor and $|Y|$ is the volume element half-length. Again equating kernels, and dividing by $|Y|$, [27].

$$\rho Dw_i/Dt = \partial \mu_{ji}/\partial x_j + e_{ijk}\tau_{jk} \qquad \text{(A 23)}$$

This is the second equation of motion or Cauchy's Second Law.

The equation of continuity is

$$\frac{D}{Dt} \int v_i = 0 \qquad \text{(A 24)}$$

For simple shear of an incompressible fluid, Equation A 24 can be simplified to

$$dv_j/dx_j = 0 \qquad \text{(A 25)}$$

which has the analogy

$$dw_j/dx_j = 0 \qquad \text{(A 26)}$$

The constitutive equations for the fluid with couple and yield stresses are defined after Valanis and Sun [63] as

$$\tau^s_{ij} = -p\delta_{ij} - s^2(\partial v_i/\partial x_j + \partial v_j/\partial x_i) + \tau_y(1 - \delta_{ij}) \text{ for } \tau_{ij} \geq \tau_y \qquad \text{(A 27a)}$$

$$\tau^s_{ij} - p\delta_{ij}, \ \partial v_i/\partial x_j = 0 \text{ for } \tau_{ij} < \tau_y \qquad \text{(A 27b)}$$

$$\mu_{ij} = 4\eta \partial w_j/\partial x_i + 4\eta' \partial w_i/\partial x_j \qquad \text{(A 28)}$$

where τ^s_{ij} is the symmetric part of the stress tensor, p is the static pressure, δ_{ij} is Kronecker's delta, s^2 is the coefficient of viscosity, τ_y is the yield stress, and η and η' are the couple stress coefficients.

From Equation A 26, it can be seen that the left hand side of Equation A 23 is zero. Rephrasing Equation A 23 in terms of some

dummy indices,

$$\partial \mathcal{K}_{rl} / \partial x_r + e_{lrk} \tau_{rk} = 0, \qquad \text{(A 29)}$$

premultiplying by e_{ijl} and converting the cyclic permutation number product into equivalent Kronecker's deltas [26]

$$e_{ijl} \partial \mathcal{K}_{rl} / \partial x_r + (\delta_{ri}\delta_{kj} - \delta_{rj}\delta_{ki}) \tau_{rk} = 0 \qquad \text{(A 30)}$$

or

$$e_{ijl} \partial \mathcal{K}_{rl} / \partial x_r = 2 \tau^{A}_{ji} \qquad \text{(A 31)}$$

where $\tau^{A}_{ij} = \frac{1}{2} (\tau_{ij} - \tau_{ji})$ is the antisymmetric part of the stress tensor.

Combining Equations A 20, A 24, and A 31, with $\tau_{ji} = \tau^{A}_{ji} + \tau^{s}_{ji}$.

$$\partial \tau^{s}_{ji} / \partial x_j + \tfrac{1}{2} e_{ijl} \partial^2 \mathcal{K}_{rl} / \partial x_r \partial x_j = 0 \qquad \text{(A 32)}$$

Substituting Equations A 27a, b, and A 28.

$$-\partial p/\partial x_i - s^2 \partial^2 v_j / \partial x_i \partial x_j - s^2 \partial^2 v_i / \partial x_j^2 +$$

$$2e_{ijl}(\eta \partial^3 w_l / \partial^2 x_r \partial x_j - \eta' \partial^3 w_r / \partial x_r \partial x_l$$

$$\partial x_j) = 0 \qquad \text{for } \tau_{ij} \geq \tau_y \qquad \text{(A 33a)}$$

$$\partial v_i / \partial x_j = 0 \qquad \text{for } \tau_{ij} < \tau_y \qquad \text{(A 33b)}$$

The second and fifth terms in Equation A 33a may be eliminated by rearranging the order of differentiation and using Equations A 25 and A 26. Substituting the vorticity tensor, W_{ij}, from Equation A 21

$$-\partial p/\partial x_i - s^2 \partial^2 v_i / \partial x_j^2 + 2\eta\, e_{ijl}(\tfrac{1}{2} e_{irs} \partial^3 W_{rs} / \partial x_r^2 \partial x_j) = 0 \qquad \text{(A 34)}$$

or in terms of the Kronecker's deltas

$$-\partial p/\partial x_i - s^2\partial^2 v_i/\partial x_j^2 + \eta(\delta_{jr}\delta_{1s} - \delta_{js}\delta_{r1})\partial^3 W_{rs}/\partial x_r^2\,\partial x_j = 0 \qquad \text{(A 35)}$$

$$-\partial p/\partial x_i - s^2\partial^2 v_i/\partial x_j^2 + \eta(\partial^3 W_{j1}/\partial x^2\partial x_j - \partial^3 W_{1j}/\partial x_r^2\partial x_j = 0 \qquad \text{(A 36)}$$

Since $w_{ij} = -w_{ji}$, Equation A 36 becomes

$$-\partial p/\partial x_i - s^2\partial^2 v_i/\partial x_j^2 + 2\eta\partial^3 W_{j1}/\partial x_r^2\partial x_j \qquad \text{(A 37)}$$

Substituting Equation A 21 to obtain the differential equation in velocity,

$$-\partial p/\partial x_i - s^2\partial^2 v_i/\partial x_j^2 + \eta\partial^4 v_1/\partial x_r^2\partial x_j^2 - \eta\partial^4 v_j/\partial x_r^2\partial x_j\partial x_1 = 0 \qquad \text{(A 38)}$$

where the fourth term may be removed by the use of Equation A 25. A convenient way to convert Equation A 38 into the cylindrical coordinates needed to solve the problem of Poiseuille flow is to first express it in vector notation

$$-\nabla p - s^2\nabla^2 v + \eta\nabla^4 v = 0 \qquad \text{(A 39a)}$$

$$-\nabla p + \nabla^2(\eta\nabla^2 v - s^2 v) = 0 \qquad \text{(A 39b)}$$

Now formally stating the conditions for Poiseuille flow,

$$v_r = v_\theta = 0, \qquad v_z = v \qquad \text{(A 40)}$$

$$\partial p/\partial r = \partial p/\partial\theta = 0, \qquad \partial p/\partial z = dp/dz \qquad \text{(A 41)}$$

$$\tau_{r\theta} = \tau_{\theta z} = 0, \quad \tau_{rz} = \tau \quad \text{for } \tau_r \geq \tau_y \qquad \text{(A 42)}$$

and applying this to Equation A 39 in cylindrical coordinates,

$$-dp/dz + 1/r\ d/dr \left[r\ d/dr\ (\eta \nabla^2 v - s^2 v) \right] = 0$$

$$\text{for} \qquad \tau \geq \tau_y \qquad \text{(A 43a)}$$

$$dv/dr = 0 \qquad \text{for} \qquad \tau < \tau_y \qquad \text{(A 43b)}$$

For steady state flow, the pressure drop is independent of axial location. Let

$$-dp/dz = \Delta p/L = k \qquad \text{(A 44)}$$

Integrating Equation A 43a with respect to r, followed by division by r, and substituting Equation A 44,

$$-s^2\ dv/dr + \tau_y + \eta\ d/dr\ \nabla^2 v = -kr/2 + c_1/r$$

$$\text{for} \qquad \tau \geq \tau_y \qquad \text{(A 45a)}$$

$$dv/dr = 0 \qquad \text{for} \qquad \tau < \tau_y \qquad \text{(A 45b)}$$

Since the right hand side of Equation A 45a may not become infinite at the centerline, c_1 must equal zero.

$$d/dr\,\eta \nabla^2 v - s^2 dv/dr = -kr/2 - \tau_y \qquad \text{for} \quad \tau \geq \tau_y \qquad \text{(A 46a)}$$

$$v = \text{constant} \qquad \text{for} \quad \tau < \tau_y \qquad \text{(A 46b)}$$

Equation 46a may be integrated with respect to r, and the final nabla expanded to give

$$\frac{\eta}{r} \left[d/dr\ (r\ dv/dr) \right] - s^2 v = -kr^2/4 - \tau_y r + C_2 \qquad \text{(A 47)}$$

Let $x = r/R$ and form the indicated derivatives to get, upon some rearrangement,

$$x^2 \frac{d^2v}{dx^2} + x \frac{dv}{dx} - \alpha^2 x^2 v - \beta x^4 + \gamma x^3 - \delta x^2 = 0 \qquad \text{(A 48)}$$

where $\alpha^2 = s^2R^2/\eta$, $\beta = \Delta p R^4/4 \eta L$, $\gamma = \tau_y R^3/\eta$, and $\delta = C_2R^2/\eta$.

Assume a series solution of the form:

$$v = \sum_{i=0}^{\infty} a_i x^i \qquad \text{(A 49)}$$

so

$$dv/dx = \sum_{i=0}^{\infty} (i+1)\, a_{i+1}\, x^i \qquad \text{(A 50)}$$

$$d^2v/dx^2 = \sum_{i=0}^{\infty} (i+2)(i+1)\, a_{i+2}\, x^i \qquad \text{(A 51)}$$

When these Equations are substituted into Equation A 43,

$$\left\{ \sum_{i=0}^{\infty} \left[(i+2)(i+1)\, a_{i+2} - \alpha^2 a_i + (i+2)\, a_{i+2} \right] x^{i+2} \right\} + a_1 x$$

$$\beta x^4 + \gamma x^3 - \delta x^2 = 0 \qquad \text{(A 52)}$$

Let $j = i + 2$.

$$a_1 x - \beta x^4 + \gamma x^3 - \delta x^2 + \sum_{j=2}^{\infty} (j^2 a_j - \alpha^2 a_j - 2)\, x^j + 0 \qquad \text{(A 53)}$$

Expanding some of the series terms to allow evaluation of like coefficients.

$$a_1 x + (4a_2 - \alpha^2 a_0 - \delta)\, x^2 + (9a_3 - \alpha^2 a_1 + \gamma)\, x^3 + (16a_4 - \alpha^2 a_2 - \beta)\, x^4 + \sum_{j=5}^{\infty} (j^2 a_j - \alpha^2 a_j - 2)\, x^j = 0 \qquad \text{(A 54)}$$

The unknown coefficients can now be obtained:

$$a_1 = 0 \qquad \text{(A 55a)}$$

$$a_2 = (\alpha^2 a_0 + \delta)/4 \qquad \text{(A 55b)}$$

$$a_3 = (\alpha^2 a_1 - \gamma)/3^2 = -\gamma/3^2 \qquad \text{(A 55c)}$$

$$a_4 = (\alpha^2 a_2 + \beta)/4^2 = \left[\alpha^2 (\alpha^2 a_0 + \delta)/4 + \beta\right]/4^2 \qquad \text{(A 55d)}$$

$$a_n = \alpha^2 a_{n-2}/n^2 \qquad n \geq 5 \qquad \text{(A 55e)}$$

$$v = a_o + (\alpha^2 a_o + \delta)\, x^2/4 - \gamma\left[x^3/3^2 + \alpha^2 x^5/3^2 5^2 + \alpha^4 x^7/3^2 5^2 7^2 + \ldots\right]$$

$$+\left[\alpha^2(\alpha^2 a_o + \delta)/4 + \beta\right]\left[x^4/4^2 + \alpha^2 x^6/4^2 6^2 + \alpha^4 x^6/4^2 6^2 8^2 + \ldots\right]$$

for $\tau \geq \tau_y$ (A 56a)

v = constant for $\tau < \tau_y$ (A 56b)

The infinite series in Equation A 56a, b can be expressed in terms of more familiar functions. Consider the modified Bessel function of zero order [1]:

$$I_o(\alpha x) = \sum_{k=0}^{\infty} \frac{(\alpha x/2)^{2k}}{k!\, k!} \qquad \text{(A 57a)}$$

$$= 1 + \frac{\alpha^2 x^2}{2^2} + \frac{\alpha^4 x^4}{2^2 4^2} + \frac{\alpha^6 x^6}{2^2 4^2 6^2} + \frac{\alpha^8 x^8}{2^2 4^2 6^2 8^2} \qquad \text{(A 57b)}$$

$$= \frac{\alpha^4}{4}\left[\frac{4}{\alpha^4} + \frac{x^2}{\alpha^2} + \frac{x^4}{4^2} + \frac{\alpha^2 x^6}{4^2 6^2} + \frac{\alpha^4 x^8}{4^2 6^2 8^2} + \ldots\right] \qquad \text{(A 57c)}$$

Therefore

$$\left[\frac{x^4}{4^2} + \frac{\alpha^2 x^6}{4^2 6^2} + \frac{\alpha^4 x^8}{4^2 6^2 8^2} + \ldots\right] = \frac{4}{\alpha^4} \mathbf{L}_o(\alpha x) - \frac{4}{\alpha^4} - \frac{x^2}{\alpha^2} \qquad \text{(A 58)}$$

Consider the modified Struve function of zero order [2]:

$$\mathbf{L}_o(\alpha x) = \sum_{k=0}^{\infty} \frac{(\alpha x/2)^{2k+1}}{\left[\Gamma(k+3/2)\right]^2} \qquad \text{(A 59a)}$$

$$= \frac{2}{\sqrt{\pi}}\left(\alpha x + \frac{\alpha^3 x^3}{3^2} + \frac{\alpha^5 x^5}{3^2 5^2} + \frac{\alpha^7 x^7}{3^2 5^2 7^2} + \ldots\right) \qquad \text{(A 59b)}$$

$$= \frac{2\alpha^3}{\sqrt{\pi}}\left(\frac{x}{\alpha^2} + \frac{x^3}{3^2} + \frac{\alpha^2 x^5}{3^2 5^2} + \frac{\alpha^4 x^7}{3^2 5^2 7^2} + \ldots\right) \qquad \text{(A 59c)}$$

Therefore

$$\left[\frac{x^3}{3^2}+\frac{\alpha^2 x^5}{3^2 5^2}+\frac{\alpha^4 x^7}{3^2 5^2 7^2}+\ldots\right]=\frac{\pi}{2\alpha^3}\,L_0(\alpha x)-\frac{x}{\alpha^2} \qquad \text{(A 60)}$$

Combining Equations A 56, A 58, and A 60

$$v = a_0 + (\alpha^2 a_0 + \delta)\, x^2/4 - \gamma\left[\pi/2\alpha^3 L_0(\alpha x) - x/\alpha^2\right] + \left[\alpha^2(\alpha^2 a_0+\delta)/4 + \beta\right]$$

$$\left[4/\alpha^4 I_0(\alpha x) - 4/\alpha^4 - x^2/\alpha^2\right] \qquad \text{(A 61)}$$

Still undetermined are two constants, a_0 and δ which contains the unknown quantity, c_2. Consider the appropriate boundary conditions. Assuming no slip at the wall,

$$v = 0 \qquad \text{at } x = 1 \qquad \text{(A 62)}$$

From symmetry considerations.

$$dv/dx = 0 \qquad \text{at } x = 0 \qquad \text{(A 63)}$$

From the vanishing of the couple stress at the wall [63] ,

$$\eta\,\frac{d^2v}{dx^2} - \eta'/x\; dv/dx = 0 \qquad \text{at } x = 1 \qquad \text{(A 64)}$$

The first and second derivatives of v are [2, 47]

$$dv/dx = 1/2\,(\alpha^2 a_0+\delta)x - \gamma\left[\pi/2\alpha^2\,(L_1(\alpha x) + 2/\pi) - 1/\alpha^2\right] +$$

$$\left[\alpha^2(\alpha^2 a_0+\delta)/4 + \beta\right]\left[4/\alpha^3 I_1(\alpha x) - 2x/\alpha^2\right] \qquad \text{(A 65)}$$

$$d^2v/dx^2 = (\alpha^2 a_0+\delta)/2 - \gamma\,\pi/2\alpha\left[L_0(\alpha x) - L_1(\alpha x)/\alpha x\right]$$

$$+\left[\alpha^2(\alpha^2 a_0+\delta)/4 + \beta\right]\left[4(\alpha I_0(\alpha x) - I_1(\alpha x)/x)/\alpha^3 - 2/\alpha^2\right] \qquad \text{(A 66)}$$

Applying Equation A 62 to Equation A 61,

$$o = a_o + (\alpha^2 a_o + \delta)/4 - \gamma\left[\pi L_o(\alpha)/2\alpha^3 - 1/\alpha^2\right]$$

$$+ \left[\alpha^4 a_o/4 + \alpha^2\delta/4 + \beta\right]\left[4I_o(\alpha)/\alpha^4 - 4/\alpha^4 - 1/\alpha^2\right] \qquad \text{(A 67)}$$

Multiplying by α^2 and combining terms involving a_o and δ,

$$\alpha^2 a_o I_o(\alpha) + (I_o(\alpha)-1)\delta = \gamma\left[\pi L_o(\alpha)/2\alpha - 1\right] + \beta\left[1 - 4(I_o(\alpha)-1)/\alpha^2\right] \qquad \text{(A 68)}$$

Equation A 63 is solved identically. Let $\bar{\eta} = \eta'/\eta$, and apply Equation A 64 to Equation A 66 and A 67,

$$(\alpha^2 a_o + \delta)/2 - \pi\gamma\left[L_o(\alpha) - L_1(\alpha)/\alpha\right]/2\alpha + \left[\alpha^4 a_o/4 + \alpha^2\delta/4 + \beta\right]$$

$$\left[4I_o(\alpha)/\alpha^2 - 4I_1(\alpha)/\alpha^3 - 2/\alpha^2\right] - \bar{\eta}\,(\alpha^2 a_o + \delta)/2 + \gamma\pi\bar{\eta}L_1(\alpha)/2\alpha^2$$

$$+\left[\alpha^4 a_o/4 + \alpha^2\delta/4 + \beta\right]\left[2\bar{\eta}/\alpha^2 - 4\bar{\eta}/\alpha^3\, I_1(\alpha)\right] = 0 \qquad \text{(A 69)}$$

or, combining terms in ao and δ,

$$\alpha^2 a_o + \delta = \frac{\gamma\pi\left(L_o(\alpha) - (1+\bar{\eta})L_1(\alpha)/\alpha\right)}{2\alpha\left(I_o(\alpha) - (1+\bar{\eta})I_1(\alpha)/\alpha\right)} - \frac{4\beta}{\alpha^2}$$

$$\left[1 - \frac{1-\bar{\eta}}{2\left(I_o(\alpha) - (1+\bar{\eta})I_1(\alpha)/\alpha\right)}\right] \qquad \text{(A 70)}$$

Multiply Equation A 70 by $I_o(\alpha)$ and subtract form Equation A 68,

$$\delta = \gamma\left[1 - \pi\left(L_o(\alpha) - \frac{L_o(\alpha) - (1+\bar{\eta})L_1(\alpha)/\alpha}{1 - (1+\bar{\eta})I_1(\alpha)/\alpha\, I_o(\alpha)}\right)/2\alpha\right]$$

$$-\beta\left[1 + 4/\alpha^2 - \frac{2\,(1-\bar{\eta})}{\alpha^2\,(1 - (1+\bar{\eta})I_1(\alpha)/\alpha\, I_o(\alpha))}\right] \qquad \text{(A 71)}$$

Combining Equation A 70 and A 71, and solving for a_o,

$$a_o = \frac{\beta}{\alpha^2}\left[1 + \frac{2(1-\bar{\eta})\,(1-I_o(\alpha))}{\alpha^2(I_o(\alpha)-(1+\bar{\eta})I_1(\alpha)/\alpha)}\right]$$

$$-\frac{\gamma}{\alpha^2}\left[1 - \frac{\pi}{2\alpha}\left(L_o(\alpha) + \frac{(1-I_o(\alpha)(L_o(\alpha)-(1+\bar{\eta})L_1(\alpha)/\alpha)}{I_o(\alpha)-(1+\bar{\eta})I_1(\alpha)/\alpha}\right)\right] \quad \text{(A 72)}$$

The velocity profile can now be written in terms of known parameters

$$v = \frac{\beta}{\alpha^2}\left[1 - x^2 + \frac{2\,(1-\bar{\eta})(I_o(\alpha x)-I_o(\alpha))}{\alpha^2(I_o(\alpha)-(1+\bar{\eta})I_1(\alpha)/\alpha)}\right]$$

$$-\frac{\gamma}{\alpha}\left[1-x + \frac{\pi}{2\alpha}\left(L_o(\alpha x)-L_o(\alpha)-(I_o(\alpha x)-I_o(\alpha)\right.\right.$$

$$\left.\left.\frac{L_o(\alpha)-(1+\bar{\eta})L_1(\alpha)/\alpha}{I_o(\alpha)-(1+\bar{\eta})I_1(\alpha)/\alpha}\right)\right]$$

$$\text{for} \quad \tau \geq \tau_y \quad \text{(A 73a)}$$

$$v = \text{constant} \quad \text{for} \quad \tau < \tau_y \quad \text{(A 73b)}$$

Let $\tau_w = \Delta\, pD/4L$, and substitute system parameters for β and γ;

$$v = \frac{\tau_w R}{2s^2}\left[1 - \frac{r^2}{R} + A\left(I_o(\alpha r/R)-I_o(\alpha)\right)\right]$$

$$-\frac{\tau_y R}{s^2}\left[1 - \frac{r}{R} + \frac{\pi}{2\alpha}\left(L_o(\alpha r/R)-L_o(\alpha)-B(I_o(\alpha r/R)-I_o(\alpha))\right)\right]$$

$$\text{for} \quad \tau \geq \tau_y \quad \text{(A 74a)}$$

$$v = \text{constant} \quad \text{for} \quad \tau < \tau_y \quad \text{(A 74b)}$$

where A and B are given by

$$A = 2(1-\bar{\eta})/(\alpha^2(I_o(\alpha) - (1+\bar{\eta})I_1(\alpha)/\alpha)) \quad \text{(A 74c)}$$

$$B = (L_o(\alpha) - (1+\bar{\eta})L_1(\alpha)/\alpha)/(I_o(\alpha)-(1+\bar{\eta})I_1(\alpha)/\alpha) \quad \text{(A 74d)}$$

3. The Viscosity of A Suspension of RBC's

The presence of red blood cells in blood is the chief factor which makes blood viscosity higher than plasma viscosity. The presence of suspended material is known to elevate viscosity. Assuming that the inertia terms in the Navier-Stokes equation are negligible, it can be shown [37] that a random suspension of rigid spheres elevates viscosity according to Einstein's equation

$$\mu_{app} = \mu_{liquid}(1 + 2.5\ \emptyset_{spheres}) \qquad \text{(A 75)}$$

without altering the non-Newtonian behavior at moderate shear rates. The supposition made is equivalent to assuming that the particle density is equal to the liquid density and that particle migration in the velocity field is negligible. These assumptions are approximately correct for blood flow.

However, the assumption of rigid spheres is quite inappropriate. Taylor [62] has shown that for non-rigid spheres, Einstein's equation must be modified to

$$\mu_{app} = \mu_{liquid}\ (1 + 2.5\ \emptyset_{spheres}\ (\mu_{drop} + .4\ \mu_{liquid})/\ (\mu_{drop} + \mu_{liquid})) \qquad \text{(A 76)}$$

Since the internal viscosity of an RBC is reported to be in the range of 1-6 cp. [19] this correction is not negligible.

The biconcave shape of the RBC should not effect the applicability of the analysis since Kynch [37] has shown that spheres with holes drilled through them behave as rigid spheres of the same diameter. However, the orientation of the non-spherical RBC's in the velocity field would make it seem as if a suspension of different size spheres were present. Roscoe [51] has shown that a mixture of rigid

sphere sizes gives

$$\mu_{app} = \mu_{liquid} / (1 - \phi_{spheres})^{2.5} \qquad \text{(A 77)}$$

where $\phi_{spheres}$ must be 1.35 times the actual volume fraction if the spheres are large enough to entrap a significant amount of liquid in a closest packed structure.

Numerous other assumptions can be made and Rutgers [54] has compiled about a hundred different equations for suspensions which have been derived or been empirically fit to data.

A form of the Einstein's equation which has been found appropriate for blood is in the reciprocal of concentration, which implies a mixture of non-spherical particles. The equation is

$$\mu_{app} = \mu_{plasma} / (1 - \Omega \phi) \qquad \text{(A 78)}$$

where

$$\Omega = 0.07\ e^{2.49\phi} + (1107/T)\ e^{-1.65\phi} \qquad \text{(A 79)}$$

and T is the absolute temperature in ^{o} Kelvin. This has been found by Charm and Kurland [12] to have an average accuracy of within 1.5% between ϕ = 0.1 - 0.6 and 10^{o}C to 37^{o}C.

Equation A 78 and all other equations above do not consider particle-particle interactions nor the ability of the particles to rotate. The equations merely represent the increased resistance to flow of a fluid in which micro-regions of plug flow are established.

In the turbulence model, particle-particle interactions will be accounted for by a yield stress and the rotation of the RBC's will be modeled as constant diameter eddies.

4. The Fluid with Particulate Turbulence

The equation of motion must be derived which describes a fluid with particulate turbulence in it. Following turbulence theory, it is assumed that the instantaneous velocity at any point can be mathematically separated into a time-averaged component, $\bar{v}$, and a fluctuating component, v',

$$v = \bar{v} + v' \qquad \text{(A 80)}$$

Equation A 83 can be transformed into (see Hinze [84], for example)

$$\eta\dot{\gamma} + \rho \overrightarrow{v_r v_z} = -\Delta pr/2L \qquad \text{(A 81)}$$

where $\eta\dot{\gamma}$ is the shear stress of the laminar flow and $-\rho \overrightarrow{v_r v_z}$ is a statistical correlation called the Reynold's stress in turbulence theory. This equation is applicable to flow with any type of disturbance in it. Assumptions made in the derivation of Equation A 81 are angular symmetry and that neither the magnitude of $\bar{v}_z$ nor its fluctuations vary in the axial direction. These assumptions are valid for flow in a constant radius viscometer tube and are not far in error for flow in vessels with low taper.

For whole blood, it is assumed that RBC's rotate in the velocity field in the tube at an angular velocity, ω, which varies with radial position (see Figure 15). Velocity fluctuations are produced tangential to the rotating RBC's and are therefore equal to the radius of an RBC, ℓ, times its angular velocity

$$v'(r) = \ell\, \omega(r) \qquad \text{(A 82)}$$

FIGURE 15

FLUCTUATIONS DUE TO A SPHERE ROTATING IN A SHEAR FIELD

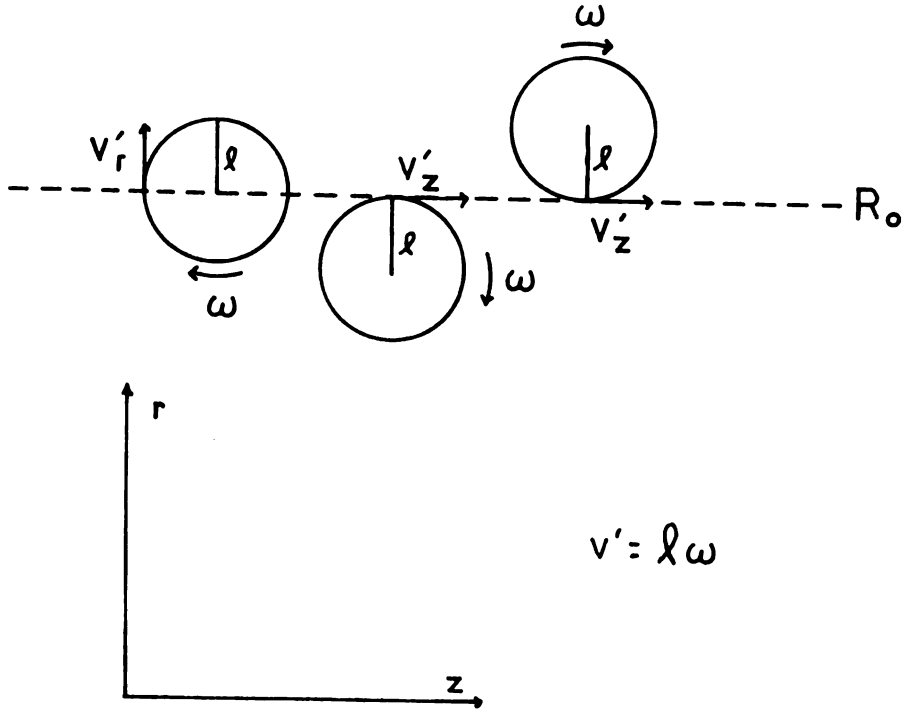

The fluctuations in the radial direction at radius R_0 are proportional to the cell tangential velocity at radius R_0 and to the percentage of cells

$$v_r'(R_0) \propto H \ell \omega(R_0) \qquad \text{(A 83)}$$

while the fluctuations in the axial direction at radius R_0 are proportional to the tangential velocities at radii $R_0 + \ell$ and $R_0 - \ell$ and to the percentage of cells

$$v_z'(R_0) \propto H \ell (\omega(R_0 - \ell) + \omega(R_0 + \ell))/2 \qquad \text{(A 84)}$$

It is assumed that the rate of rotation is proportional to the mean velocity difference on the opposite sides of the cell

$$\omega(R_0) \propto (\bar{v}(R_0 + \ell) - \bar{v}(R_0 - \ell))/2\ell \qquad \text{(A 85)}$$

Next, the mean velocity is expanded in a Taylor's series since the dimensions of a red blood cell are small

$$\bar{v}(R_0 + y) \propto \bar{v}(R_0) + y\,\partial\bar{v}(R_0)/\partial r + y^2/2\,\partial^2\bar{v}(R_0)/\partial r^2 + \ldots \qquad \text{(A 86)}$$

Therefore, from Equation A 85 and A 86,

$$\omega(R_0) \propto \partial\bar{v}/\partial r \qquad \text{(A 87)}$$

And, from Equations A 84, A 85 and A 86,

$$v_z' \propto H \ell\, \partial\bar{v}/\partial r \qquad \text{(A 88)}$$

Equations A 83 and A 87 combine to give

$$v_r' \propto H \ell \left|d\bar{v}/dr\right|$$

since the sign of v_r' depends on whether ℓ is considered in a positive or negative direction and on the magnitude of dv/dr only.

Therefore, the equivalent of the turbulent Reynold's stress, τ_{Re}, is given by

$$\tau_{Re} = -\overline{\rho v_r' v_z'} = +\rho H^2 \ell^2 \epsilon \, (dv/dr)^2 \qquad \text{(A 90)}$$

where ϵ is a constant of proportionality and where the absolute value sign has been removed utilizing the fact that dv/dr is everywhere negative for axial flow in a tube. This result is identical with Prandl's mixing length theory or Taylor's vorticity transport theory, except that this model states that ℓ is not a function of position from the wall as is assumed in the other models.

Now it is assumed that the shear stress due to laminar flow is linear with the strain rate, except that the yield stress must be exceeded before strain begins.

$$\tau_\ell = -\mu \, d\bar{v}/dr + \tau_y \qquad \tau_\ell \geq \tau_y \qquad \text{(A 91a)}$$

$$d\bar{v}/dr = 0 \qquad \tau_\ell < \tau_y \qquad \text{(A 91b)}$$

where μ is the viscosity of a suspension of RBC's in plasma. See the section on the viscosity of a suspension of RBC's in this appendix for further explanation. Then Equation A 81, A 90, and A 91a can be combined to

$$\tau_y - \mu \, d\bar{v}/dr + \rho H^2 \ell^2 \epsilon \, (d\bar{v}/dr)^2 = \Delta pr/2L \qquad \text{(A 92)}$$

This can be solved by the quadratic equation for $d\bar{v}/dr$.

$$dv/dr = \frac{(\mu - \sqrt{\mu^2 - 4\rho H^2 \ell^2 \epsilon \, (\tau_y - \Delta pr/2L)})}{2\rho H^2 \ell^2 \epsilon} \qquad \text{(A 93)}$$

where the negative value for the square root has been chosen because it is desired that dv/dr go to zero as $-\Delta pr/2L$ goes to the yield stress.

Equation A 93 predicts that the maximum velocity gradient will exist at the wall boundary.

However this implies that the maximum turbulence, which is proportional to the velocity gradient squared, also occurs at the wall boundary. This is impossible since a RBC physically cannot be centered at the wall and the model depicted in Figure 15 requires one at that position to impart a velocity fluctuation in radial direction. In order to correct for this inconsistency, a region which is approximately one red blood cell in width will be included next to the wall in the model. In this region, the turbulence will be presumed to fall linearly from the value given by Equation A 93 to zero at the wall. The model then consists of three regions expressed mathematically as

$$-\Delta pr/2L - \tau_y = -\mu(dv/dr) + \beta(R-r) \quad \text{for } R \geq r > b \qquad \text{(A 94a)}$$

$$-\Delta pr/2L - \tau_y = -\mu(dv/dr) + \rho H^2 \ell^2 \epsilon \quad (dv/dr)^2$$

$$\text{for } b \geq r \geq \tau_y R/\tau_w \qquad \text{(A 94b)}$$

$$0 = dv/dr \qquad \tau_y R/\tau_w > r \geq 0 \qquad \text{(A 94c)}$$

where

$$\beta(r-b) = \rho H^2 \ell^2 \epsilon \quad (dv/dr)^2 \; r=b \qquad \text{(A 95)}$$

so that the turbulence is a continuous quantity. Integration of Equation A 94a yields

$$v = (\Delta p/2L-\beta)\, r^2/2\mu + (\tau_y + \beta R)\, r/\mu + C_2 \quad \text{for } R \geq r > b \qquad \text{(A 96)}$$

Since the velocity goes to zero at the wall, the constant C_2 can be determined.

$$v = (\Delta p/2L-\beta)(r^2-R^2)/2\mu + (\tau_y + \beta R)(r-R)/\mu \quad \text{for } R \geq r > b$$

(A 97)

From Equation A 93, which was derived from the equivalent of Equation A 94b,

$$(dv/dr)^2_{r=b} = 2\psi^2 - 2\psi(\varphi^2 - 2\tau_y\psi/\mu - \Delta p\psi b/\mu L)^{1/2} - 2\tau_y\psi/\mu - \Delta pb\psi/\mu L \qquad \text{(A 98)}$$

where $\psi = \mu/2\beta H^2\ell^2\epsilon$.

Therefore from Equations A 95 and A 98,

$$\beta = (\psi/\mu - \mu(\varphi^2 - 2\tau_y\psi/\mu - \Delta p\psi b/\mu L)^{1/2} - \tau_y - \Delta pb/2L)/(R-b) \qquad \text{(A 99)}$$

so that β can be expressed in terms of system constants.

Integration of Equation A 93 yields

$$v = \psi r + \frac{2\mu L}{3\psi\,\Delta p}(\varphi^2 - 2\tau_y\psi/\mu - \Delta pr\psi/\mu L)^{3/2} + C_3 \quad \text{for } b \geq r \geq \tau_y R/\tau_w \qquad \text{(A 100)}$$

It is necessary that the velocity at radius b given by Equation A 100 agrees with the velocity given by Equation A 97 so that the velocity is not discontinuous. This allows the constant C_3 to be determined.

$$v = \psi(r-b) + \frac{2\mu L}{3\psi\,\Delta p}\left[(\varphi^2 - 2\tau_y\psi/\mu - \Delta pr\psi/\mu L)^{3/2} - (\varphi^2 - 2\tau_y\psi/\mu - \Delta pb\psi/\mu L)^{3/2}\right] + (\Delta p/2L - \beta)(b^2 - R^2)/2\mu + (\tau_y + \beta R)(b-R)/\mu \quad \text{for } b \geq r \geq \tau_y R/\tau_w \qquad \text{(A 101)}$$

It is necessary that dv/dr goes to zero at the yield radius, $r = \tau_y R/\tau_w$. It can be seen from Equation A 93 that this condition is identically satisfied. The (constant) velocity in the center of the tube can then be found by using Equation A 101

$$v = \psi(\tau_y R/\tau_w - b) + \frac{2\mu L}{3\psi\Delta p}\left[\psi^3 - (\psi^2 - 2\tau_y\psi/\mu + 2\tau_w b\psi/\mu R)^{3/2}\right] + (\Delta p/2L - \beta)(b^2-R^2)/2\mu + (\tau_y + \beta R)(b-R)/\mu \quad \text{for } \tau_y R/\tau_w > r \geq 0 \qquad \text{(A 102)}$$

The flow rate in a tube can then be found by integration of the velocity profiles

$$Q = 2\pi\left(\int_0^{\tau_y R/\tau_w} vrdr + \int_{\tau_y R/\tau_w}^{b} vrdr + \int_b^R vrdr\right) \qquad \text{(A 103)}$$

where the velocities are given by Equations A 102, A 101 and A 97, respectively. By integration and collection of like terms,

$$\begin{aligned} Q/2\pi R^3 = {} & \tau_w(1/8 - b/24R - b^2/24R^2 - b^3/24R^3)/\mu + \\ & \tau_y(-1/8 + b/24R + b^2/24R^2 + b^3/24R^3)/\mu + \\ & \psi(\tau_y^3/6\tau_w^3 - b^3/24R^3 - b^2/24R^2 - b/24R - \\ & 1/24 - \psi^2\mu\tau_y^2/6\tau_w^3 + \psi^3\mu^2\tau_y/15\tau_w^3 - \\ & \psi^4\mu^3/105\tau_w^3 + (1 - 2\tau_y/\psi\mu + \tau_w b/ \\ & \psi\mu R)^{\frac{1}{2}}\left[\psi(-8\tau_y^3/105\tau_w^3 - 4b\tau_y^2/105\,\tau_w^2 R - \right. \\ & b^2\tau_y/35\,\tau_w R^2 + b^3/56R^3 + b^2/24R^2 + b/24R + \\ & 1/24) + \psi^2\mu(4\tau_y^2/35\tau_w^3 + 4b\tau_y/105\tau_w^2 R + \\ & b^2/70\tau_w R^2) - \psi^3\mu^2(2\tau_y/35\tau_w^3 + b/105\tau_w^2 R) \\ & \left. + \psi^4\mu^3/105\tau_w^3\right] \end{aligned} \qquad \text{(A 104)}$$

For the term involving the square root, the order of magnitude of $\psi\mu$ is estimated

$$\psi\mu = \mu^2/2\rho \quad H^2\ell^2\epsilon = (.06)^2/(2)(1)(\tfrac{1}{2})^2(3\times10^{-4})^2(1)$$

$$= 8 \times 10^4 \text{ dyne/cm}^2 \qquad \text{(A 105)}$$

and it can be seen that $2(b\tau'_w/R - \tau'_y)/\psi\mu$ is small in comparison to unity for any reasonable values of τ'_w. Therefore, the square root in Equation A 104 may be expanded in a Taylor's series

$$(1 + 2(\tau'_w b/R - \tau_y)/\psi\mu)^{\frac{1}{2}} = 1 + (b\tau_w/R - \tau_y)/\psi\mu -$$

$$(\tau_w b/R - \tau_y)^2/2\psi^2\mu^2 + (\tau_w b/R - \tau_y)^3/2\psi^3\mu^3 -$$

$$5(\tau'_w b/R - \tau'_y)^4/8\psi^4\mu^4 + 7(\tau'_w b/R - \tau_y)^5/8\psi^5\mu^5 -$$

$$21(\tau_w b/R - \tau_y)^6/16\psi^6\mu^6 + \ldots \qquad \text{(A 106)}$$

Inserting Equation A 106 in Equation A 104 and collecting like terms,

$$Q/2\pi R^3 = \bar{U} = \Big[\tau_w/8 - \tau_y/6 + \tau_y^4/24\,\tau_w^3 + (\tau_w^2(b^5/80R^5$$

$$-b^4/48R^4 - b^3/48R^3 - b^2/48R^2) + \tau_y\tau_w(b^3/24R^3 + b^2/24R^2$$

$$+ b/24R) - \tau_y^2\ (b^3/48R^3 + b^2/48R^2 + b/48R$$

$$1/48) + \tau_y^5/120\tau_w^3)/\psi\mu + (\tau_w^3(-b^6/48R^6 +$$

$$b^5/48R^5 + b^4/48R^4 + b^3/48R^3) + \tau_w^2\tau_y(3b^5/80R^5$$

$$-b^4/16R^4 - b^3/16R^3 - b^2/16R^2) + \tau_w\tau_y^2\ (b^3/16R^3$$

$$+ b^2/16R^2 + b/16R) - \tau_y^3(b^3/48R^3 + b^2/48R^2 +$$

$$b/48R + 1/48) + \tau_y^6/240\tau_w^3)/\psi^2\mu^2 + \ldots\Big]/\mu \qquad \text{(A 107)}$$

As the particle size approaches molecular dimensions, Equation A 107 should reduce to the fluid model without turbulence, that is, the Bingham model. This is the case for, as ℓ approaches zero, ψ becomes infinite and all terms on the right hand side drop out except the first three.

APPENDIX B

APPENDIX B

COMPUTER PROGRAMS

Several computer programs were used to analyze raw data and to aid in the preparation of graphs. The programs were written in FORTRAN IV compatible with a CDC 6500 computer. Use on other computers requires deck modification.

The first program below was used to get yield stress and viscosity parameters from the flow-pressure data described in the experimental section. This is program TYNS.

The second program listed, PROFILE, was used to generate Figure 3. It utilizes double precision functions BES0, BES1, STRU0, and STRU1 for the modified Bessel and Struve functions.

The last program listed, ZERLI, was used to generate Figure 4. It also utilizes the double precision functions listed with the previous program.

```
      PROGRAM TYNS (INPUT,OUTPUT)
      DIMENSION W(60),X(60),Y(60),Z(60),U(60,13),T(13),A(13),B(13),C(13)
     X,D(13),TW(60,13),SUT(13),STT(13),COEF(13),ES(13),VAR(13),RP@(60)
   98 FORMAT (*       WITH       A=1/8.S.S      B=-2.SQRT(T)/7.S.S      C=-
     XT.T.T.T/168.S.S      D=T/6.S.S  *)
   99 FORMAT (* *,T50,* MISCELLANEOUS INFORMATION.    *,T1,I3,2X,A5,A6,
     X4X,A6,4X,I1,9X,F10.6)
  100 FORMAT (8F10.5)
  101 FORMAT (5X,*A=*,E13.6,* B=*,E13.6,* C=*,E13.6,* D=*,E13.6)
  103 FORMAT(*0FOR SAMPLE *,A5,* WITH*,I3,* POINTS, HEMATOCRIT= *,A6,
     X*AND PH= *,A6,*, THE RESULTS IN TUBE *,I2,* ARE:↓↓ *)
  104 FORMAT (*+*,60X,*MINIMUM % VARIANCE IS IN CALCULATION *,I2)
  105 FORMAT (5X,*S=*,F10.5,* SXS=*,F10.7,* TAU YIELD=*,3F10.5)
  106 FORMAT (*1 DATA FIT TO        U=A.TW +B.SQRT TW +C/TW.TW.TW +D *)
  107 FORMAT (*9*,4X,F10.6,3X,F10.6,3X,F10.6,3X,F10.6,3X,F10.6,3X,F10.4)
  108 FORMAT (9X,*HT CM*,10X,*Q*,11X,*TW*,11X,*U*,11X,*UBEST*,9X,*DP/Q*)
  110 FORMAT (1X,13F10.5)
  111 FORMAT (* % VARIANCE, THEN S, THEN YIELD STRESS, THEN VISCOSITY:*)
  112 FORMAT (*-  CALCULATED U VALUES ↓↓ *)
  113 FORMAT (*+*,80X,* UBEST % VARIANCE=*,F10.6)
C*************************************************************************
C         W=H(CM H2O)  X=TW(DYNE/CM2)  Y=U(1/SEC)  Z=Q(ML/MIN)
C         CALCULATE BEST COEFFICIENTS WHICH AGREE WITH CASSON EQUATION FORM
C         THEN ESTIMATE YIELD STRESS VALUES FROM THESE NUMBERS.
C*************************************************************************
      PRINT 106
      PRINT 98
  115 READ 99,N,SAMP,PH,CT,NTUBE,DENS
      IF (N) 400,400,119
  119 READ 100,EL,DELMV
      R=DELMV/10.0586
      Q=EL/(R+.0005462*R*R)
      R=Q*.0005462
      READ 100,(W(I),Z(I),I=1,N)
      GO TO (120,122,124,126,128,130,132,134,136),NTUBE
```

```
C        TUBE 1 BASED ON L=16.048  D=503.5                    **********
  120 DO 121 K=1,N
      W(K)=W(K)/10.0586
      W(K)=Q*W(K)+R*W(K)*W(K)-Z(K)*Z(K)*DENS/24.284
      X(K)=W(K)/1.3044
      RPM(K)=W(K)/Z(K)
  121 Y(K)=Z(K)/0.0060162
      GO TO 138
C        TUBE 2 BASED ON L=15.796  D=397.9                    **********
  122 DO 123 K=1,N
      W(K)=W(K)/10.0586
      W(K)=Q*W(K)+R*W(K)*W(K)-Z(K)*Z(K)*DENS/9.4650
      X(K)=W(K)/1.6248
      RPM(K)=W(K)/Z(K)
  123 Y(K)=Z(K)/0.0029679
      GO TO 138
C        TUBE 3 BASED ON L=15.659   D=986.2                    **********
  124 DO 125 K=1,N
      W(K)=W(K)/10.0586
      W(K)=Q*W(K)+R*W(K)*W(K)-Z(K)*Z(K)*DENS/359.51
      X(K)=W(K)/0.64979
      RPM(K)=W(K)/Z(K)
  125 Y(K)=Z(K)/0.04520
      GO TO 138
C        TUBE 4 BASED ON L=12.464  D=164.8                    **********
  126 DO 127 K=1,N
      W(K)=W(K)/10.0586
      W(K)=Q*W(K)+R*W(K)*W(K)-Z(K)*Z(K)*DENS/0.27829
      X(K)=W(K)/3.0962
      RPM(K)=W(K)/Z(K)
  127 Y(K)=Z(K)/0.00021073
      GO TO 138
C        TUBE 5 BASED ON L=12.167   D=207.3                    **********
  128 DO 129 K=1,N
      W(K)=W(K)/10.0586
      W(K)=Q*W(K)+R*W(K)*W(K)-Z(K)*Z(K)*DENS/0.69759
```

```
      X(K)=W(K)/2.4020
      RPQ(K)=W(K)/Z(K)
  129 Y(K)=Z(K)/0.00041980
      GO TO 138
C        TUBE 6 BASED ON L=10.371     D=207.3                    **********************
  130 DO 131 K=1,N
      W(K)=W(K)/10.0586
      W(K)=Q*W(K)+R*W(K)*W(K)-Z(K)*Z(K)*DENS/0.69759
      X(K)=W(K)/2.0474
      RPQ(K)=W(K)/Z(K)
  131 Y(K)=Z(K)/0.00041980
      GO TO 138
C        TUBE 7 BASED ON L=5.220     D=128.1                    **********************
  132 DO 133 K=1,N
      W(K)=W(K)/10.0586
      W(K)=Q*W(K)+R*W(K)*W(K)-Z(K)*Z(K)*DENS/0.10170
      X(K)=W(K)/1.6677
      RPQ(K)=W(K)/Z(K)
  133 Y(K)=Z(K)/0.000099046
      GO TO 138
C        TUBE 8 BASED ON L=             D=                      **********************
  134 DO 135 K=1,N
      W(K)=W(K)/10.0586
      W(K)=Q*W(K)+R*W(K)*W(K)-Z(K)*Z(K)*DENS
      X(K)=W(K)/1.
      RPQ(K)=W(K)/Z(K)
  135 Y(K)=Z(K)
      GO TO 138
C        TUBE 9 BASED ON L=9.307  D=207.3                        **********************
  136 DO 137 K=1,N
      W(K)=W(K)/10.0586
      W(K)=Q*W(K)+R*W(K)*W(K)-Z(K)*Z(K)*DENS/0.69759
      X(K)=W(K)/1.8374
      RPQ(K)=W(K)/Z(K)
  137 Y(K)=Z(K)/0.00041980
```

```
138 SXR=0     $SXM3=0     $SXY=0     $SXRY=0     $SYXM3=0     $SX32=0
    SY=0    $SX2=0      $SX=0      $SXM6=0      $SXM2=0      $SXM52=0
    DO 140 I=1,N
    X2=X(I)*X(I)
    X3=X2*X(I)
    SX=SX+X(I)
    SX2=SX2+X2
    SY=SY+Y(I)
    SXY=SXY+X(I)*Y(I)
    SXR=SXR+SQRT(X(I))
    SXRY=SXRY+Y(I)*SQRT(X(I))
    SYXM3=SYXM3+Y(I)/X3
    SXM6=SXM6+1./X3/X3
    SX32=SX32+SQRT(X3)
    SXM2=SXM2+1./X2
    SXM52=SXM52+1./SQRT(X3*X2)
    IF (X(I)) 300,140,140
140 SXM3=SXM3+1./X3
    Z1=SX*SXY-SY*SX2
    Z2=SX2*SXR-SX*SX32
    Z3=SX2*SXM3-SX*SXM2
    Z4=SX2*N-SX*SX
    Z5=SY*SX32-SX*SXRY
    Z6=SX*SX-SXR*SX32
    Z7=SX*SXM52-SXM3*SX32
    Z8=SX*SXR-N*SX32
    Z9=SY*SXM2-SX*SYXM3
    Z10=SX*SXM52-SXR*SXM2
    Z11=SX*SXM6-SXM3*SXM2
    Z12=SX*SXM3-N*SXM2
    W1=Z2*Z5-Z1*Z6
    W2=Z2*Z7-Z3*Z6
    W3=Z2*Z8-Z4*Z6
    W4=Z1*Z10-Z2*Z9
    W5=Z3*Z10-Z2*Z11
    W6=Z4*Z10-Z2*Z12
```

```
      D1=ABS ((W2*W4-W1*W5)/(W3*W5-W2*W6))
      C1=-ABS ((W3*D1+W1)/W2)
      B1=-ABS ((Z1+Z3*C1+Z4*D1)/Z2)
      A1=ABS ((SY-B1*SXR-C1*SXM3-N*D1)/SX)
      PRINT 103,SAMP,N,CT,PH,NTUBE
      PRINT 99
      PRINT 101,A1,B1,C1,D1
      T1=49.*B1*B1/256./A1/A1
      T2=(-21.*C1/A1)**.25
      T3=0.75*D1/A1
      S2=0.125/A1
      S=SQRT(S2)
      PRINT 105,S,S2,T1,T2,T3
C*****************************************************************************
C        PRINT OUT DP, Q, TW, U, BEST FIT U, DP/Q, AND VARIANCE.
C*****************************************************************************
      PRINT 108
      GSUM=0.
      DO 160 L=1,N
      G=A1*X(L)+B1*SQRT(X(L))+C1*X(L)**(-3)+D1
      GSUM=GSUM+((G-Y(L))/G)**2
      PRINT 107,W(L),Z(L),X(L),Y(L),G,RPQ(L)
  160 CONTINUE
      GSUM=GSUM/(N-2)
      PRINT 113,GSUM
C*****************************************************************************
C        COVERING A RANGE OF YIELD VALUES, FIND BEST FIT FOR S
C        AND CALCULATE VARIANCE FOR EACH CASE.
C*****************************************************************************
      TINC=0.0
      IF (T1) 191,191,189
  189 IF (T1-.012) 190,190,191
  190 TDEL=T1/12.
      GO TO 200
  191 TDEL=0.001
  200 VARMI=100.0
```

```
      DO 201 I=1,13
      SUT(I)=0.
      STT(I)=0.
      T(I)=TDEL*(I-1)+TINC
      A(I)=0.125
      B(I)=-SQRT(T(I))/3.5
      C(I)=-1./168.*T(I)**4
      D(I)=T(I)/6.
      DO 202 L=1,N
      TW(L,1)=A(I)*X(L)+B(I)*SQRT(X(L))+C(1)*X(L)**(-3)+D(I)
      SUT(I)=SUT(I)+TW(L,I)*Y(L)
  202 STT(I)=STT(I)+TW(L,I)*TW(L,I)
      COEF(I)=ABS ( STT(I)/SUT(I))
  201 ES(I)=SQRT(COEF(I))
      DO 210 I=1,13
      A(I)=A(I)/COEF(I)
      B(I)=B(I)/COEF(I)
      C(I)=C(I)/COEF(I)
      D(I)=D(I)/COEF(I)
C*****************************************************************************
C        COMPUTER PICKS YIELD STRESS AND S WHICH GIVE MINIMUM VARIANCE.
C*****************************************************************************
      VAR(I)=0.
      DO 209 L=1,N
      U(L,I)=TW(L,I)/COEF(I)
  209 VAR(I)=VAR(I)+((U(L,I)-Y(L))/U(L,I))**2
      COEF(I)=COEF(I)*100.
      VAR(I)=VAR(I)/(N-2)
      IF (VAR(I)-VARMI) 220,210,210
  220 NVAR=I
      VARMI=VAR(I)
  210 CONTINUE
      IF (NVAR-13) 222,221,222
  221 TINC=TINC+12*TDEL
      GO TO 200
  222 CONTINUE
```

```
      PRINT 112
      PRINT 110,((U(K,I),I=1,13),K=1,N)
      PRINT 111
      PRINT 104,NVAR
      PRINT 110,VAR,ES,T,COEF
      PRINT 101,A(NVAR),B(NVAR),C(NVAR),D(NVAR)
  300 GO TO 115
  400 END
```



```
      PROGRAM PROFILE ( INPUT, OUTPUT)
      DOUBLE EB,A,B,C,D,X,Y,PI
  202 FORMAT (1X,4D20.12,2E20.12)
      TY=0.04
      PI=3.14159265358979323850D0
      DO 110 L=1,4
      GO TO (10,11,12,15),L
   10 TW=TY
      GO TO 19
   11 TW=0.0404
      GO TO 19
   12 TW=0.4
      GO TO 19
   15 TW=400.
      DO 100 I=1,3
      GO TO (20,22,26),I
   20 EB=-1.00D0
      GO TO 29
   22 EB=0.0D0
```

```
      GO TO 29
   26 EB=1.00D0
   29 CONTINUE
      GO TO (30,31,32,33),J
   30 A=0.01D0
      GO TO 39
   31 A=1.0D0
      GO TO 39
   32 A=5.0D0
      GO TO 39
   33 A=100.0D0
   39 CONTINUE
      B=BES0(A)-(1.0D0-EB)*BES1(A)/A
      C=2.0D0*(1.0D0-EB)/A/A/B
      D=(STRU0(A)-(1.0D0-EB)*STRU1(A)/A)/B
      DO 80 K=1,14
      GO TO (40,41,42,43,44,45,46,47,48,49,50,51,52,53),K
   40 X=1.00D0
      GO TO 55
   41 X=.999D0
      GO TO 55
   42 X=0.95D0
      GO TO 55
   43 X=.900D0
      GO TO 55
   44 X=0.800D0
      GO TO 55
   45 X=0.700D0
      GO TO 55
   46 X=0.600D0
      GO TO 55
   47 X=0.500D0
      GO TO 55
   48 X=0.400D0
      GO TO 55
   49 X=0.300D0
```

```
      GO TO 55
   50 X=0.200D0
      GO TO 55
   51 X=0.100D0
      GO TO 55
   52 X=0.010D0
      GO TO 55
   53 X=0.10D-9
   55 CONTINUE
      Y=A*X
      V=TW/2.0D0*((1.0D0-X*X)+C*(BES0(Y)-BES0(A))-TY*(1.0D0-X+PI/2.0D0
     2/A*((STRU0(Y)-STRU0(A))-D*(BES0(Y)-BES0(A))))
   80 PRINT 202,X,Y,C,D,V
  100 CONTINUE
  110 CONTINUE
      END
0000000000000000000000
      DOUBLE PRECISION FUNCTION BES0(X)
      DOUBLE TBES,X,Z,XI,TERM
      TBES=1.00D0
      IF (X.EQ.0.0D0) GO TO 10
      Z=X*X/4.D0
      TERM=Z
      XI=2.0D0
    4 TBES=TBES+TERM
      IF (TERM.LT.1.D-25) GO TO 10
      TERM=TERM*Z/XI/XI
      XI=XI+1.0D0
      GO TO 4
   10 BES0=TBES
      RETURN
      END
      DOUBLE PRECISION FUNCTION BES1(X)
      DOUBLE TBES,X,Z,XI,TERM,ELIM,XJ
      Z=X*X/4.0D0
      TBES=X/2.0D0
```

```
      IF ( X.EQ.0.0D0) GO TO 10
      ELIM=Z*1.0D-25
      XI=2.0D0
      TERM=TBES*Z/XI
    4 TBES=TBES+TERM
      IF (TERM.LT.ELIM) GO TO 10
      XJ=XI
      XI=XI+1.0D0
      TERM=TERM*Z/XI/XJ
      GO TO 4
   10 BES1=TBES
      RETURN
      END
      DOUBLE PRECISION FUNCTION STRU0(X)
      DOUBLE X,Z,TSTRU,ELIM,XI,TERM
      Z=X*X
      TSTRU=X
      IF (X.EQ.0.0D0) GO TO 10
      ELIM=Z*1.0D-25
      XI=3.0D0
      TERM=TSTRU
    4 TERM=TERM*Z/XI/XI
      TSTRU=TSTRU+TERM
      IF (TERM.LT.ELIM) GO TO 10
      XI=XI+2.0D0
      GO TO 4
   10 STRU0=TSTRU*0.63661977236758134306553500D00
      RETURN
      END
      DOUBLE PRECISION FUNCTION STRU1(X)
      DOUBLE X,Z,TSTRU,ELIM,XI,TERM,XJ
      Z=X*X
      XI=3.0D0
      TSTRU=Z/XI
      IF (X.EQ.0.0D0) GO TO 10
      ELIM=Z*Z*1.0D-25
```

```
      TERM=TSTRU
    4 XJ=XI
      XI=XI+2.0D0
      TERM=TERM*Z/XI/XJ
      TSTRU=TSTRU+TERM
      IF (TERM.GT.ELIM) GO TO 4
   10 STRU1=TSTRU*0.63661977236758134306553500D00
      RETURN
      END
0000000000000000000000
```

```
      PROGRAM ZERLI (INPUT,OUTPUT)
      DOUBLE A,B,C,D,EB,XI,TNUM,TDEN
    9 FORMAT(6X,*EB*,11X,*A*,14X,*TW/TY*)
   10 FORMAT (1X,2D12.5,E20.10)
      PI=3.14159265359
      PRINT 9
      DO 100 I=1,21
      XI=1
      EB=(XI-11.0D0)/10.0D0
      DO 90 J=1,10
      GO TO (30,31,32,33,34,35,36,37,38,39),J
   30 A=1.0D-10
      GO TO 40
   31 A=1.0D-2
      GO TO 40
   32 A=1.0D-1
      GO TO 40
   33 A=0.50D0
      GO TO 40
```

```
   34 A=1.0D0
      GO TO 40
   35 A=5.0D0
      GO TO 40
   36 A=10.0D0
      GO TO 40
   37 A=20.0D0
      GO TO 40
   38 A=1.0D2
      GO TO 40
   39 A=2.0D2
   40 CONTINUE
      B=1.0D0-(1.0D0+EB)*STRU1(A)/STRU0(A)/A
      C=1.0D0-(1.0D0+EB)*BES1(A)/BES0(A)/A
      D=1.0D0-1.0D0/BES0(A)
      TNUM=1.0D0-(PI*STRU0(A)/2.0D0/A)*(1.0D0-(B/C)*D)
      TDEN=0.50D0-(1.0D0-EB)*D/A/A/C
      TWOTY=TNUM/TDEN
   90 PRINT 10,EB,A,TWOTY
  100 CONTINUE
      END
0000000000000000000000
```

APPENDIX C

APPENDIX C

EXPERIMENTAL DATA

Experimental data in the form of pressure drops at certain flow rates were gathered from the flow-pressure apparatus described previously. These data can be converted to τ_w versus $\bar{U}$ data such as shown in Figure 2. The data in this form have been fit by least squares analysis using computer program TYNS, which is listed in Appendix B. The statistically best values for the Casson viscosity and yield stress are listed below for each run. Table 4 gives the results for the ionic additives experiments. Table 5 gives the results for the active hyperemia experiments.

TABLE 4

RESULTS OF IONIC ADDITIVES EXPERIMENTS

Run	Hct	pH	Tube Number	Additive*	Age, Days	Casson Viscosity, cp	Casson Yield Stress, dynes/cm^2
24A	43.5	7.455	6	C	0	3.985	.081
24B	42.0	7.45	6	K	0	3.845	.029
24C	43.75	7.38	6	Mg	0	3.958	.027
24D	38.0	7.400	6	Na + K	1	4.371	.032
24E	38.5	7.37	6	K	1	4.089	.039
24F	36.0	7.37D	6	C	1	3.412	.047
27A	39.0	7.33	6	C	0	3.703	.021
27B	39.0	7.29	6	K	0	3.673	.029
30A	32.0	7.32D	6	C	0	3.066	.005
30B	35.0	7.29D	6	Na + K	0	3.255	.013
30C	31.2	7.28D	6	K	0	3.137	.005
30D	30.3	7.25D	6	Na	0	2.437	.041
30E	29.5	7.23D	6	C	0	2.624	.007
32A	33.75	7.54D	4	C	0	3.401	.033
32C	33.0	7.43D	4	K	0	3.189	.005
32E	33.75	7.42D	4	Mg	1	3.238	.000
32F	33.5	7.36D	4	C	1	3.225	.0067
33A	42.0	7.44	4	C	0	2.833	.025
33B	41.0	7.44	4	Na + K	0	2.572	.017
33C	40.4	7.42D	4	Na	0	3.044	.005
33D	39.75	7.39D	4	K	0	2.871	.022
35A	35.5	7.28D	4	C	0	3.702	.000
35B	33.3	7.25D	4	Na + K	0	3.310	.005
35E	36.0	7.14D	4	C	1	3.559	.002
35F	36.0	7.18D	4	K	1	3.496	.000
36A	22.0	7.42	9	C	0	2.532	.005
36B	22.2	7.45D	9	Na + K	0	2.452	.001

TABLE 4 (Cont'd.)

Run	Hct	pH	Tube Number	Additive*	Age, Days	Casson Viscosity, cp	Casson Yield Stress, dynes/cm^2
36C	23.5	7.41D	9	K	0	2.357	.0046
36D	23.6	7.42D	9	Na	0	2.386	.016
36E	22.0	7.38D	9	Mg	1	2.459	.004
36F	23.0	7.29D	9	Ca	1	2.594	.0043
36G	23.0	7.33D	9	C	1	2.583	.0001
37A	41.3	7.41D	9	Na + K	0	4.171	.065
37B	40.7	7.44	9	C, SH	0	3.823	.023
37C	40.8	7.46	9	K	0	3.302	.125
37D	40.3	7.385	9	Ca	1	3.353	.006
37E	40.3	7.40D	9	Mg	1	3.240	.007
37F	39.8	7.38D	9	C	1	3.445	.084
39A	39.8	7.31D	9	C	0	2.854	.002
39B	39.0	7.27	9	Ca	0	2.427	.008
39C	40.5	7.340	9	Na + K	1	3.617	.021
39D	43.0	7.338	9	K	1	3.514	.002
39E	38.9	7.33	9	C	1	2.451	.004
40B	43.5	7.585	9	K	1	1.648	.003
40C	42.9	7.59	9	Na + K	1	1.720	.001
40D	41.6	7.57	9	C	1	1.570	.004
40E	40.9	7.60	9	Mg	1	1.594	.002
40F	40.4	7.53	9	Ca	1	1.496	.004
41A	22.3	7.41D	9	Na + K	1	2.843	.024
41B	22.0	7.34	9	C	1	2.428	.034
41C	21.8	7.28D	9	Ca	2	2.693	.013
41D	22.5	7.28D	9	Mg	2	2.160	.034
41E	23.0	7.24D	9	C	2	2.611	.025
42A	35.9	7.40	9	Mg	1	2.818	.068
42B	32.6	7.33	9	Ca	1	2.403	.080
42C	34.0	7.49D	9	C	1	2.328	.104

TABLE 4 (Cont'd.)

Run	Hct	pH	Tube Number	Additive*	Age, Days	Casson Viscosity, cp	Casson Yield Stress, dynes/cm^2
42E	32.0	7.458	9	Na	2	3.432	.004
42F	33.0	7.33	9	C	2	3.208	.011
42G	34.3	7.34	9	3Na + K,SH	3	3.274	.051
42H	32.5	7.27D	9	C,SH	3	2.745	.019
42I	34.0	7.28D	9	Na + K,SH	3	3.108	.014
43A	29.9	7.40D	9	Ca	0	2.562	.020
43B	30.0	7.47D	9	Mg	0	2.448	.020
43C	34.5	7.40D	9	C	0	2.873	.000
43D	30.9	7.45D	9	Na	1	3.297	.013
43E	30.1	7.41D	9	C	1	3.471	.000
43F	30.9	7.39	9	3Na + K	1	3.268	.001
45A	35.75	7.29D	9	Ca	3	5.227	.008
45B	33.5	7.33	9	Mg	3	3.877	.018
45C	35.0	7.26D	9	C	3	5.016	.005
46A	36.0	7.35D	9	C	1	3.681	.017
46B	35.9	7.36D	9	Ca	1	3.195	.017
47A	39.9	7.36D	9	Mg	1	2.990	.009
47B	39.6	7.275	9	Ca	1	2.901	.007
47C	39.7	7.255	9	C	1	3.200	.011
51B	30.5	8.07	2	OH	1	2.836	.035
51C	33.25	7.46	2	C	1	3.280	.033
51D	37.0	6.74	2	H	1	3.171	.054
52A	44.5	7.115	2	H	0	3.695	.043
52B	38.0	7.845	2	OH	0	3.460	.006
52C	38.4	7.53	2	C	0	2.552	.040
52D	40.5	7.515	2	C	1	4.196	.004
52E	44.4	7.115	2	H	1	3.511	.069
52F	39.9	7.79D	2	OH	1	4.071	.006
53A	30.3	7.09	2	H	0	3.212	.021
53B	23.0	7.94	2	OH	0	2.601	.004

TABLE 4 (Cont'd.)

Run	Hct	pH	Tube Number	Additive*	Age, Days	Casson Viscosity, cp	Casson Yield Stress, dynes/cm^2
53C	25.5	7.545	2	C	0	2.585	.0029
53D	25.7	7.57	2	Na	0	2.521	.038
54A	34.0	7.86	2	OH	0	2.649	.025
54B	36.0	7.43D	2	C	0	3.350	.010
54C	38.3	7.19	2	H	0	2.955	.021
54D	33.3	7.855	2	OH,SH	2	3.845	.002
54E	36.0	7.395	2	C	2	3.680	.037
54F	39.2	7.04	2	H	2	3.790	.047
55A	33.8	7.42D	2	C	0	2.654	.038
55C	32.0	7.71	2	OH	0	2.660	.039
55D	35.8	7.01	2	H	0	2.356	.080
56A	22.1	7.385	2	C	1	2.470	.013
56B	22.0	7.755	2	OH	1	2.566	.012
56C	24.0	7.00D	2	H	1	2.469	.018
58A	38.3	6.93	2	H	0	3.324	.062
58B	35.6	7.38	2	C	0	3.287	.049
58C	34.5	7.77D	2	OH	0	3.703	.045
58D	35.0	7.765	2	OH	1	4.876	.058
58E	37.0	7.455	2	C	1	4.922	.040
60A	35.2	7.365	2	C	2	3.569	.033
60B	38.2	7.06	2	H	2	3.427	.032
60C	32.8	7.785D	2	OH	2	3.098	.022
63C	36.7	7.395	2	3Na + K	1	3.936	.073
63D	36.0	7.395	2	C	1	3.317	.051
65C	37.0	7.28	2	C	1	3.548	.077
65D	38.1	6.97	2	H	1	3.158	.096

* Notation

C	Isotonic dialysate solution added
Ca	Isotonic calcium chloride added
D	pH fell more than 0.1 during experiment
H	Isotonic 1:1 hydrochloric acid in dialysate added
K	Isotonic potassium chloride added
Mg	Isotonic magnesium chloride added
Na	Isotonic sodium chloride added
Na + K	Isotonic 1:1 potassium chloride in sodium chloride added
3Na + K	Isotonic 1:3 potassium chloride in sodium chloride added
OH	Isotonic 1:3 sodium hydroxide in dialysate added
SH	Slightly hemolysed

TABLE 5

RESULTS OF ACTIVE HYPEREMIA EXPERIMENTS

Desig.	Hct	pH	Tube Number	Status*	Casson Viscosity, cp	Casson Yield Stress, dynes/cm^2
25A	52.0	7.37	6	S	5.810	.142
25I	45.0	7.52	6	C	5.445	.086
31A	42.0	7.10	2	S, E	3.090	.065
31B	40.0	7.23	2	S	3.519	.020
31C	39.0	7.31	2	C	3.845	.018
38A	41.0	7.33D	9	S	3.356	.027
38B	35.0	7.46D	9	C	3.999	.006
44A	36.9	7.17D	9	S	3.224	.023
44B	33.0	7.35D	9	C	3.361	.000
48A	33.9	7.36D	9	C	4.036	.001
48B	38.0	7.17D	9	S	4.296	.001
59A	34.7	7.465	2	C	3.368	.071
59B	34.35	7.345	2	S	3.269	.069
62A	55.5	7.457	2	C, UO	6.721	.064
62B	59.0	7.350	2	S, UO	5.929	.104
63A	-	7.320	2	C, UO	6.694	.076
63B	52.0	7.195	2	S, UO	4.735	.086
64A	51.0	7.295	2	C, UO	5.254	.034
64B	51.7	7.155	2	S, UO	5.443	.099
65A	46.0	7.175	2	S, UO	4.903	.169
65B	44.3	7.30D	2	C, UO	3.988	.108

* Notation

C	Collected during control period
E	Collected at end of experiment
S	Collected during stimulation (active hyperemia)
UO	Collected under mineral oil

TABLE 6

SUMMARY OF TREATMENT EFFECTS

Treatment[a]	N	Effect of Treatment on Yield Stress, DYNE/CM2			Effect of Treatment on Viscosity, % of Control		
		Average	95% Confidence Limits		Average	95% Confidence Limits	
			Lower	Upper		Lower	Upper
Na	6	.0121	-.0124	.0366	97.81	89.08	106.54
3Na + K	3	.0183	-.0210	.0576	110.69	75.09	146.29
Na + K	10	.0026	-.0093	.0145	115.19	103.48	126.90
K	11	.0011	-.0240	.0262	104.28	93.67	114.89
Ca	10	-.0085	-.0278	.0108	95.53	90.36	100.70
Mg	10	-.0130	-.0358	.0098	94.40	85.85	102.95
H	11	.0187	.0058	.0316	101.35	89.22	113.48
OH	11	-.0042	-.0156	.0072	100.53	90.42	110.64
STIM	10	.0276	.0090	.0462	96.71	86.40	107.02

(a) Abbreviations explained in Tables 4 and 5.

APPENDIX D

APPENDIX D

NOTATION

ENGLISH UPPER CASE

A	term grouping
B	term grouping
C_1, C_2, C_3	constants of integration
D	tube diameter, domain
F	force on body
H	hematocrit
I_0, I_1	modified Bessel functions
L	torque, tube length
L_0, L_1	modified Struve functions
M	couple stress tensor
P	momentum
Q	flow rate
R	tube radius
S	surface area
T	tra c tion
$\bar{U}$	flow rate = $4Q/\pi D^3$
V	volume
W	vorticity tensor
Y	volume element half-length

ENGLISH LOWER CASE

a	constant coefficient, power series coefficient
b	constant coefficient, marginal gap width
e_{ijk}	cyclic permutation number

ENGLISH LOWER CASE (Cont'd.)

f	fluidity
g	acceleration of gravity
h	difference in manometer leg levels
k	pressure gradient = $-\Delta p/L$
l	RBC radius
n	normal vector
p	pressure
r	radial position, recorder reading
s	coefficient of viscosity
v	velocity vector, velocity
w	vorticity vector
x	coordinate axis direction
y	position vector

GREEK

α	term grouping ($\alpha^2 = s^2 R^2 / \eta$)
$\bar{\alpha}$	term grouping ($\bar{\alpha}^2 = \mu R^2/\eta$)
β	term coefficient
γ	term coefficient
δ	term coefficient
δ_{ij}	Kronecker's delta
Δ	difference of
ϵ	proportionality constant
η	couple stress coefficient
η'	couple stress coefficient
$\bar{\eta}$	term grouping ($\bar{\eta} = \eta'/\eta$)

GREEK (Cont'd.)

λ	volume measure = 1 mm^3
μ	coefficient of viscosity
μ_{ij}	couple stress
π	3.14159265.....
ρ	fluid density
Σ	summation of
τ	stress, shear stress
$\emptyset$	volume fraction
ψ	term grouping = $\mu/2\rho H^2 \ell^2 \epsilon$
$\sim$	Einstein Law function

OTHER

$\partial y/\partial x$	partial derivative of y
dy/dx	total derivative of y
Dy/Dt	Eulerian derivative of y
∇	gradient of
∇^2	nabla operator
$\int$	integral
$\oint$	surface integral
$\|\|$	magnitude of vector

SUBSCRIPTS

i	coordinate index, iteration index
j	coordinate index, iteration index
k	coordinate index
l	coordinate index
r	coordinate index

SUBSCRIPTS (Cont'd.)

s	coordinate index
w	wall value
y	yield value

SUPERSCRIPTS

A	antisymmetric
s	symmetric
-	time average
'	fluctuating
$\bar{U}$	velocity average (tube diameters/time)
$\bar{\eta}$	term grouping = η'/η

BIBLIOGRAPHY

BIBLIOGRAPHY

1. Abramowitz, M., and Stegun, I. A. Handbook of Mathematical Functions, U.S. Government Printing Office, Washington, D.C., 375, 376 (1965).

2. Ibid., 496, 498.

3. Benis, A. M., Sc.D. Thesis, Massachusetts Institute of Technology, 97, 99, 212 (1964).

4. Ibid., 17.

5. Ibid., 54, 55.

6. Bingham, E. C. and Roepke, R. R., J. Gen. Physiol., 28, 79 (1944).

7. Bird, R. B., Stewart, W. E., and Lightfoot, E. N., Transport Phenomena, Wiley and Sons, New York, 85, (1966).

8. Bugliarello, G., and Hayden, J. W., Trans. Soc. Rheol., 7, 209 (1963).

9. Carrier, O., Ph.D. Thesis, U. Miss. Med. Center (1964).

10. Casson, N., in Rheology of Disperse Systems, ed. C. C. Mill, Pergamon Press, New York, 84-104 (1959).

11. Charm, S., and Kurland, G., Nature, 206, 617 (1965).

12. Charm, S., and Kurland, G., Biorheology, 3, 163-164 (1966).

13. Cokelet, G. R., et al., Trans. Soc. Rheol., 7, 303 (1963).

14. Conn, R. B., Current Therapy, 1969, W. B. Saunders, Philadelphia, cover, (1969).

15. Copley, A. L., in Flow Properties of Blood and Other Biological Systems, ed. Copley, A. L., and Stainsby, G., Pergamon Press, New York, 110-113 (1960).

16. Davidsohn, I., and Henry, J. B., Clinical Diagnosis by Laboratory Methods, W. B. Saunders, Philadelphia, 1263 (1969).

17. de Raedt, M., et. al., J. Appl. Physiol., 26, 469 (1969).

BIBLIOGRAPHY (Cont'd.)

18. Dintenfass, L., Nature, 213, 179 (1967).

19. Dintenfass, L., Nature, 219, 956 (1968).

20. Eringen, A. C., Mechanics of Continua, Wiley and Sons, New York 98 (1967).

21. Fahraeus, R., and Lindqvist, T., Am. J. Physiol., 96, 562 (1930).

22. Fishman, A. P., and Richards, D. W., Circulation of the Blood, Oxford U. Press, New York, 86, (1964).

23. Frasher, W. G., et al., J. Appl. Physiol., 25, 751 (1968).

24. Fung, Y. C., A First Course in Continuum Mechanics, Prentiss-Hall, Englewood Cliffs, New Jersey, 52 (1969).

25. Ibid., 190.

26. Ibid., 26.

27. Ibid., 40.

28. Gilinson, P. J. Jr., et. al., Trans. Soc. Rheol., 7, 319 (1963).

29. Guest, G. M., and Siler, V. E., J. Lab. Clin. Med., 19, 757-767 (1934).

30. Haddy, F. J., and Scott, J. B., Physiology 501 Class Notes, Mich. St. U., adapted from Annual Rev. Pharmacol., 6, 50 (1966).

31. Haddy, F. J., and Scott, J. B., in Electrolytes and Cardiavascular Diseases, ed. E. Bajusz, Karger, New York, 383-393 (1965).

32. Haynes, R. T., and Burton, A. C., Am. J. Physiol., 197, 943 (1959).

33. Hershey, D., and Sung, J. C., J. Appl. Physiol., 21, 27 (1966).

34. Hinze, J. O., Turbulence, McGraw-Hill, New York, 14-19 (1959).

35. Hodgman, C. D., ed., Handbook of Chemistry and Physics, Chem. Rubber Co., Cleveland, Ohio, 2251, 2257 (1963).

36. Jacobs, H. R., Biorheology, 3, 117 (1966).

37. Kynch, G. J., Brit. J. Appl. Physics, 5, 53, 55-511 (1954).

BIBLIOGRAPHY (Cont'd.)

38. Masin, J. G., Biorheology, in process.

39. Mayer, G. A., and Kiss, O., Am. J. Physiol., 208, 795 (1965).

40. Mayer, G. A., et. al., Biorheology, 3, 177 (1966).

41. Merrill, E. W., et. al., Biophysics J., 3, 199 (1963).

42. Merrill, E. W., et. al., Circulation Research, 18, 437 (1966).

43. Merrill, E. W., et. al., J. Appl. Physiol., 26, 1 (1969).

44. Merrill, E. W., in Biophysical Mechanisms in Vascular Homeostasis and Intravascular Thrombosis, ed. Sawyer, P. N., Appleton-Century-Crofts, New York, 121-137 (1965).

45. Merrill, E. W., and Pelletier, G. A., J. Appl. Physiol., 23, 178-182 (1967).

46. Merrill, E. W., et. al., J. Appl. Physiol., 20, 954-967 (1965).

47. Mickley, H. S., Sherwood, T. K., and Reed, C. E., Applied Mathematics in Chemical Engineering, McGraw-Hill, New York, 179 (1957).

48. Murphy, J. R., J. Lab. Clin. Med., 69, 758 (1967).

49. Nielsen, A. V., et. al., J. Appl. Physiol., 22, 1167 (1967).

50. Rand, P. W., et. al., J. Appl. Physiol., 25, 550 (1968).

51. Roscoe, R., Brit. J. Appl. Physics, 3, 267-269, (1952).

52. Rosenblum, W. I., Blood, 31, 234 (1968).

53. Roth, S. A., Ph.D. Thesis, Mich. St. U. (1970).

54. Rutgers, I. R., Rheol. Acta, Band 2, Heft 4, 305-348 (1962).

55. Schmid-Schonbein, H., and Wells, R., Science, 165, 288 (1969).

56. Scott, J. B. et. al., Federation Proc., 27, 1403 (1968).

57. Scott, J. B., et. al., Am. J. Physiol., 218, 338-345 (1970).

58. Scott Blair, G. W., Nature, 183, 613 (1959).

BIBLIOGRAPHY (Cont'd.)

59. Siegel, N. J., and Kolmen, S. N., Am. J. Physiol., 216, 707 (1969).

60. Stokes, V. K., Physics of Fluids, 9, 1709 (1966).

61. Ibid., 1710.

62. Taylor, G. I., Proc. Royal Soc., (London), A138, 41-48 (1932).

63. Valanis, K. C., and Sun, C. T., Biorheology, 6, 86 (1969).

64. Ibid., 88.

65. Ibid., 97.

66. Van Wazer, J. R., et. al., Viscosity and Flow Measurement, Wiley and Sons, New York, 201-215 (1963).

67. Ibid., 206.

68. Walder, D. N., Weaver, J. P. A., and Evans, A., Biorheology, 6, 23 (1969).

69. Wells, R. E., et. al., Clin. Res., 11, 176 (1963).

70. Whittaker, S. R. F., and Winton, F. R., J. Physiol., 78, 331-369 (1933).